Scheduling and Pricing of Energy Generation and Storage in Power Systems

Roohallah Khatami, *Student Member, IEEE*, Masood Parvania, *Member, IEEE*, Pramod Khargonekar, *Fellow, IEEE*

***Abstract*—This paper proposes a fundamental model for continuous-time scheduling and marginal pricing of energy generation and storage in day-ahead power systems operation. The paper begins with formulating the economic operation problem of power systems with generating units and energy storage (ES) devices as a continuous-time optimal control problem, where the Lagrange multiplier trajectory associated with the continuous-time power balance constraint is proven to be the marginal price of energy generation and storage. The marginal price is calculated in closed-form, which reveals that in addition to the incremental cost rates of generating units, the marginal price embeds the financial ES charging offers and discharging bids that are defined as incremental charging utility and incremental discharging cost rates. This paper shows that the adjoint function associated with the ES state equation establishes a temporal dependence between the marginal prices during the ES charge and discharge states. A function space-based method is developed to solve the proposed model, which converts the continuous-time problem into a mixed-integer linear programming problem with finite dimensional decision space. The features of the proposed scheduling and pricing models are demonstrated using numerical studies conducted on the IEEE Reliability Test System.**

***Index Terms*—Continuous-time optimal control, energy storage, marginal price, mixed-integer linear programming.**

I. Introduction

ENERGY storage is considered to be the ultimate solution for the ongoing discourse over renewable energy intermittency challenge, offering flexibility to counterbalance the net-load vagaries and inheriting the advantages of both fast-ramping generation and flexible loads [1]–[3]. Energy storage (ES) represents the lossy temporal shift of electric energy that is fundamentally different from energy generation and consumption, and requires new models and market rules for integration in power systems scheduling and pricing practices.

A. Regulatory Context and Current Work

In recent years, policy makers have focused on upgrading electricity market regulations to appropriately accommodate and compensate the flexibility services provided by ES devices. To this end, FERC issued order No. 755 [4] to facilitate the participation of fast-ramping service providers, including ES devices, in regulation markets. Most recently, FERC issued a notice of proposed rulemaking [5] and required independent system operators (ISOs) and regional transmission operators to establish market participation models for ES devices to ensure that: 1) ES devices are eligible to provide the capacity, energy, and ancillary services they are technically capable of providing, 2) ES devices are able to set the market clearing price, 3) transactions are conducted in locational marginal prices, and 4) ES bidding parameters are incorporated.

In response to the FERC orders, power system operators and ISOs have been modifying their markets and operation practices to accommodate the participation of utility-scale ES devices. California ISO has been working with other stakeholders to develop the California energy storage roadmap [6], and a two-phase initiative for enhancing the ability of grid-connected ES devices to participate in their market [7]. New York ISO is embedding ES in the operation of energy, regulation, operating reserve, and capacity markets [8]. Midcontinent ISO includes ES in the regulation market and is in pursuit of enhancing market rules to spur ES deployment [9]–[11]. New England ISO allows ES to provide most of the services provided by generation and demand response resources [12].

In addition to the policy drivers, there have been notable efforts in research community to develop scheduling and pricing models for integrating ES services in power systems operation [13]–[21]. The optimal utilization of ES devices for transmission network applications using an optimal power flow model was investigated in [13]. However, the model in [13] does not optimize the coupled operation of generating units and ES, which underestimated the benefits of ES utilization in system. In [14], the centralized and distributed dispatch of ES devices are compared and the ensuing impacts on the system operation are studied. Market power mitigating role of ES is discussed in [15], and a novel interval unit commitment formulation is presented in [16] where pumped hydro storage provides both energy and reserve services in the system. In [17], high ramping capability of utility-scale battery storage is leveraged to maintain the short-term loading of transmission lines within limits in case of $K-1$ line contingencies. The authors in [18] discuss thoroughly the large-scale ES utilization challenges in power systems with high renewable integration. Although it is more common to treat ES devices as a market resource, some operators, e.g., PJM [19], consider them as a transmission asset. In [20], ES devices are considered as passive transmission assets that shift the load, and a concept analogous to financial transmission rights is developed to valuate and compensate the assets when they reach the maximum power or energy limits.

One of the promises of utility-scale ES devices is that they provide dispatch flexibility and fast ramping capability to compensate large and fast variations of load and renewable energy resources in power systems. However, the current discrete-

This work was supported in part by the U.S. Department of Energy grant DE-OE0000882, and in part by the U.S. National Science Foundation grants ECCN-1549924 and CNS-1723856.

R. Khatami and M. Parvania are with the Department of Electrical and Computer Engineering, the University of Utah, Salt Lake City, UT 84108 USA (e-mails: roohallah.khatami@utah.edu, masood.parvania@utah.edu)

P. Khargonekar is with the Department of Electrical Engineering and Computer Science, the University of California, Irvine, CA 92697 USA (e-mail: pramod.khargonekar@uci.edu).

time, e.g., hourly, market operation practices model power trajectories with piecewise constant functions and define ramping as the finite difference of discrete-time power samples, thus forcing the resources (including ES devices) to follow a linear ramp [22]. We argue that the traditional discrete-time operation models may not fully exploit the flexibility of ES devices and impede our way to optimally schedule, justly valuate, and fairly compensate the flexibility services provided by the ES devices in power systems operation. In addition, questions on how the intertemporal ES operation impacts the marginal electricity prices remain unaddressed.

B. Contribution and Paper Structure

This paper aims at developing a fundamental, analytically tractable and general model for joint scheduling and pricing of generating units and ES devices in day-ahead power systems operation. The scheduling problem is formulated as a *continuous-time optimal control problem*, which schedules for optimal continuous-time power and ramping trajectories of generating units and ES devices to supply the net-load trajectory over the scheduling horizon. The continuous-time pricing counterpart problem is formed by fixing the commitment variables of generating units to their optimal values obtained from the scheduling problem.

In addition, a function space-based method is developed to solve the proposed continuous-time problem. In the proposed solution method, the continuous-time generation and ramping trajectories of generating units as well as the energy, power and ramping trajectories of ES devices are modeled in function spaces spanned by Bernstein polynomials. The proposed method converts the continuous-time problem into a mixed integer linear programming (MILP) problem with the Bernstein coordinates of decision trajectories as decision variables. The convex hull property of Bernstein polynomials is utilized to efficiently impose the continuous-time inequality constraints, including the energy, power and ramping constraints of ES devices. A key advantage of the proposed solution method allows for full exploitation of the ES capabilities through higher-order solution spaces, while including, as a special case, the traditional discrete-time solution through the zeroth order Bernstein polynomial approximation. The other major contributions of this paper are outlined below:

- This paper defines the *continuous-time ramping trajectories* of ES devices as time derivatives of their power trajectories, capturing their ramping flexibility to supply the fast ramping requirement of net-load. In addition, the *continuous-time energy trajectories* of ES devices are modeled as integrals of the ES power trajectories, facilitating accurate modeling of continuous-time ES state of charge dynamics and constraints.
- Using the optimality conditions of the pricing problem, we prove that the Lagrange multiplier trajectory of the continuous-time power balance constraint is *continuous-time marginal price of energy generation and storage*.
- The continuous-time marginal price is calculated in closed-from, which shows that the marginal price not only depends on the incremental cost rate of generating units, but also on terms that embed the financial ES charging offers and discharging bids defined as *incremental charging utility rate* and *incremental discharging cost rate*.
- The closed-form marginal price formulas show that when a generating unit or ES device reaches the ramping limits, time derivatives of the Lagrange multiplier associated with the binding ramping constraint appears in the price formula, causing a price increase that reflects the shortage of ramping in the system.
- The adjoint function of the ES state equation is defined as *net incremental surplus of stored energy (NISSE)*, which quantifies the net surplus of incremental change in the energy stored at the ES device over the charge-discharge cycle. It is shown that *NISSE* establishes a temporal dependence between the incremental discharging cost and incremental charging utility rates of the ES device, thereby creating a temporal dependence between marginal prices during the ES charging and discharging states.

The rest of this paper is organized as follows: In section II, we formulate the proposed scheduling and pricing problems and derive the optimality conditions. The optimality conditions are utilized in Section III and IV to define and calculate the continuous-time marginal price of energy generation and storage. The proposed function space-based solution method is presented in Section V. The numerical results conducted on the IEEE Reliability Test System (RTS) are presented in Section VI, and conclusions are drawn in Section VII.

II. Proposed Scheduling and Pricing Problems

Consider the day-ahead power system operation problem where a set of K generating units and R energy storage (ES) devices are available to balance a net-load trajectory $D(t)$, over day-ahead horizon $\mathcal{T} = [0, T]$. This problem may be an ISO's problem who receives offers from generating units and ES devices in the day-ahead market, or a traditional operator's problem who owns the generation and storage assets.

The generating units are modeled by continuous-time generation trajectories and binary commitment variables that respectively form the vectors $\mathbf{G}(t) = (G_1(t), \ldots, G_K(t))^T$ and $\mathbf{I}(t) = (I_1(t), \ldots, I_K(t))^T$. Besides, the associated ramping trajectories, defined as time derivatives of the generation trajectories, are represented by $\dot{\mathbf{G}}(t) = \big(\dot{G}_1(t), \ldots, \dot{G}_K(t)\big)^T$.

The power trajectory of ES devices is decomposed into the charging and discharging components, both deemed as positive trajectories. In charging state, ES devices draw power from the grid, and vectors $\mathbf{D}^s(t) = \big(D_1^s(t), \ldots, D_R^s(t)\big)^T$ and $\dot{\mathbf{D}}^s(t) = \big(\dot{D}_1^s(t), \ldots, \dot{D}_R^s(t)\big)^T$ represent the charging power and ramping trajectories. In discharging state, ES devices supply power to the grid, and vectors $\mathbf{G}^s(t) = \big(G_1^s(t), \ldots, G_R^s(t)\big)^T$ and $\dot{\mathbf{G}}^s(t) = \big(\dot{G}_1^s(t), \ldots, \dot{G}_R^s(t)\big)^T$ denote the discharging power and ramping trajectories. The continuous-time energy trajectory of ES devices is shown by vector $\mathbf{E}^s(t) = \big(E_1^s(t), \ldots, E_R^s(t)\big)^T$.

The instantaneous operating cost function of a generating unit, denoted as $C^G\big(G_k(t), I_k(t)\big)$, includes the generation cost as well as the startup and shutdown costs of the unit. For ES devices, discharging cost function $C^S\big(G_r^s(t)\big)$ represents the cost of supplying energy back to the grid as a function of

discharging power trajectory. Also, charging utility function $U^S\big(D_r^s(t)\big)$ expresses the charging utility of ES device as a function of charging power trajectory. The cost and utility functions are expressed in dollars per unit of time.

A. Continuous-time Scheduling Problem

The continuous-time energy generation and storage scheduling problem is formulated here as an *optimal control problem*, where the generation trajectories of generating units as well as charging and discharging power and energy trajectories of ES devices are the state variables. The ramping trajectories of generating units and ES devices are the control variables. Objective of the proposed model in (1) is to minimize the total operation cost of system over the scheduling horizon $\mathcal{T}$, which is subject to the operating constraints (2)-(14):

$$\min_{\dot{\mathbf{G}}(t),\dot{\mathbf{G}}^s(t),\dot{\mathbf{D}}^s(t)} \int_{\mathcal{T}} C^G\big(\mathbf{G}(t),\mathbf{I}(t)\big)dt + \int_{\mathcal{T}} C^S\big(\mathbf{G}^s(t)\big)dt - \int_{\mathcal{T}} U^S\big(\mathbf{D}^s(t)\big)dt, \tag{1}$$

$$\frac{d\mathbf{G}(t)}{dt} = \dot{\mathbf{G}}(t), \quad t\in\mathcal{T}, \quad \big(\boldsymbol{\gamma}^G(t)\big), \tag{2}$$

$$\frac{d\mathbf{G^s}(t)}{dt} = \dot{\mathbf{G}}^s(t), \quad t\in\mathcal{T}, \quad \big(\boldsymbol{\gamma}^{s,G}(t)\big), \tag{3}$$

$$\frac{d\mathbf{D^s}(t)}{dt} = \dot{\mathbf{D}}^s(t), \quad t\in\mathcal{T}, \quad \big(\boldsymbol{\gamma}^{s,D}(t)\big), \tag{4}$$

$$\frac{d\mathbf{E^s}(t)}{dt} = \boldsymbol{\eta}^c\mathbf{D}^s(t) - \boldsymbol{\eta}^{\boldsymbol{d}^{-1}}\mathbf{G}^s(t), \ t\in\mathcal{T}, \ \big(\boldsymbol{\gamma}^{s,E}(t)\big), \tag{5}$$

$$\mathbf{1}_K^T\mathbf{G}(t)+\mathbf{1}_R^T\mathbf{G}^s(t)=D(t)+\mathbf{1}_R^T\mathbf{D}^s(t), \ t\in\mathcal{T}, \ (\lambda(t)), \tag{6}$$

$$\underline{\mathbf{G}}\mathbf{I}(t) \le \mathbf{G}(t) \le \overline{\mathbf{G}}\mathbf{I}(t), \quad t\in\mathcal{T}, \quad \big(\underline{\boldsymbol{\nu}}^G(t),\overline{\boldsymbol{\nu}}^G(t)\big), \tag{7}$$

$$0 \le \mathbf{G}^s(t) \le \overline{\mathbf{G}}^s, \quad t\in\mathcal{T}, \quad \big(\underline{\boldsymbol{\nu}}^{s,G}(t),\overline{\boldsymbol{\nu}}^{s,G}(t)\big), \tag{8}$$

$$0 \le \mathbf{D}^s(t) \le \overline{\mathbf{D}}^s, \quad t\in\mathcal{T}, \quad \big(\underline{\boldsymbol{\nu}}^{s,D}(t),\overline{\boldsymbol{\nu}}^{s,D}(t)\big), \tag{9}$$

$$\underline{\mathbf{E}}^s \le \mathbf{E}^s(t) \le \overline{\mathbf{E}}^s, \quad t\in\mathcal{T}, \quad \big(\underline{\boldsymbol{\nu}}^{s,E}(t),\overline{\boldsymbol{\nu}}^{s,E}(t)\big), \tag{10}$$

$$\underline{\dot{\mathbf{G}}}\mathbf{I}(t)+\overline{\dot{\mathbf{G}}}^{SD}\int_{t-\epsilon}^{t+\epsilon}\dot{\mathbf{I}}(t')dt' \le \dot{\mathbf{G}}(t) \le \overline{\dot{\mathbf{G}}}\mathbf{I}(t)+\overline{\dot{\mathbf{G}}}^{SU}\int_{t-\epsilon}^{t+\epsilon}\dot{\mathbf{I}}(t')dt', \quad t\in\mathcal{T}, \quad \big(\underline{\boldsymbol{\mu}}^G(t),\overline{\boldsymbol{\mu}}^G(t)\big), \tag{11}$$

$$\underline{\dot{\mathbf{G}}}^s \le \dot{\mathbf{G}}^s(t) \le \overline{\dot{\mathbf{G}}}^s, \quad t\in\mathcal{T}, \quad \big(\underline{\boldsymbol{\mu}}^{s,G}(t),\overline{\boldsymbol{\mu}}^{s,G}(t)\big), \tag{12}$$

$$\underline{\dot{\mathbf{D}}}^s \le \dot{\mathbf{D}}^s(t) \le \overline{\dot{\mathbf{D}}}^s, \quad t\in\mathcal{T}, \quad \big(\underline{\boldsymbol{\mu}}^{s,D}(t),\overline{\boldsymbol{\mu}}^{s,D}(t)\big), \tag{13}$$

$$\mathbf{G}(0)=\mathbf{G}^0, \mathbf{G}^s(0)=\mathbf{G}^{s,0}, \mathbf{D}^s(0)=\mathbf{D}^{s,0}, \mathbf{E}^s(0)=\mathbf{E}^{s,0}. \tag{14}$$

The total operation cost (1) is equal to the generation cost of generating units, $C^G\big(\mathbf{G}(t),\mathbf{I}(t)\big)=\sum_K C^G\big(G_k(t),I_k(t)\big)$, plus the total discharging cost of ES devices, $C^S\big(\mathbf{G}^s(t)\big)=\sum_R C^S\big(G_r^s(t)\big)$, minus the total charging utility of ES devices $U^S\big(\mathbf{D}^s(t)\big)=\sum_R U^S\big(D_r^s(t)\big)$. The ramping trajectories are defined in (2)-(4), and the state equation (5) controls the state of charge of ES devices in continuous-time over the scheduling horizon; $\boldsymbol{\eta}^c$ and $\boldsymbol{\eta}^d$ in (5) are diagonal $R\times R$ matrices of charging and discharging efficiencies. The continuous-time power balance constraint of the system is formulated in (6), where $\mathbf{1}_K$ and $\mathbf{1}_R$ are K and R-dimensional vectors of ones.

The power, ramping, and energy trajectories over $\mathcal{T}$ are constrained in (7)-(13), where the constant underlined and overlined terms respectively represent the minimum and maximum limits of the trajectories. In (11), $\dot{\mathbf{I}}(t)=(\dot{I}_1(t),\ldots,\dot{I}_K(t))^T$ is time derivative of the commitment variables that models the startup/shutdown of generating units, where ϵ is an infinitesimally small positive number. Constraint (11) also facilitates ramping during the startup and shutdown periods, where $\overline{\dot{\mathbf{G}}}^{SU}$ and $\overline{\dot{\mathbf{G}}}^{SD}$ are diagonal matrices of startup and shutdown ramping limits. Initial values of the state trajectories are enforced in (14), where $\mathbf{G}^0$, $\mathbf{G}^{s,0}$, $\mathbf{D}^{s,0}$, and $\mathbf{E}^{s,0}$ are vectors of constant initial values.

The parenthesis in the right-hand-sides of (2)-(13) show the adjoint and Lagrange multiplier trajectories. More specifically, $\boldsymbol{\gamma}^G(t)$, $\boldsymbol{\gamma}^{s,G}(t)$, $\boldsymbol{\gamma}^{s,D}(t)$, and $\boldsymbol{\gamma}^{s,E}(t)$ denote the adjoint trajectories associated with the state equations; $\underline{\boldsymbol{\nu}}^G(t)$, $\underline{\boldsymbol{\nu}}^{s,G}(t)$, $\underline{\boldsymbol{\nu}}^{s,D}(t)$, $\underline{\boldsymbol{\nu}}^{s,E}(t)$, $\underline{\boldsymbol{\mu}}^G(t)$, $\underline{\boldsymbol{\mu}}^{s,G}(t)$, and $\underline{\boldsymbol{\mu}}^{s,D}(t)$ denote the Lagrange multiplier trajectories associated with the minimum limit constraints, and $\overline{\boldsymbol{\nu}}^G(t)$, $\overline{\boldsymbol{\nu}}^{s,G}(t)$, $\overline{\boldsymbol{\nu}}^{s,D}(t)$, $\overline{\boldsymbol{\nu}}^{s,E}(t)$, $\overline{\boldsymbol{\mu}}^G(t)$, $\overline{\boldsymbol{\mu}}^{s,G}(t)$, and $\overline{\boldsymbol{\mu}}^{s,D}(t)$ represent the Lagrange multipliers associated with the maximum limit constraints.

B. Continuous-time Pricing Problem

Let us define the vectors of state and control variables $\mathbf{x}(t)$ and $\mathbf{u}(t)$ of the optimal control problem (1)-(14) as:

$$\mathbf{x}(t) = \left(\mathbf{G}(t);\mathbf{G}^s(t);\mathbf{D}^s(t);\mathbf{E}^s(t)\right), \tag{15}$$

$$\mathbf{u}(t) = \left(\dot{\mathbf{G}}(t);\dot{\mathbf{G}}^s(t);\dot{\mathbf{D}}^s(t)\right). \tag{16}$$

In addition, suppose that the problem (1)-(14) is solved, using the method proposed in Section V, and the optimal binary variables $\mathbf{I}^*(t)$ are calculated. We adapt the approach in [23], [24], fix the binary variables to their optimal values $\mathbf{I}^*(t)$, and formulate the continuous-time pricing problem as:

$$\min_{\mathbf{u}(t)} J = \int_{\mathcal{T}} F\left(\mathbf{x}(t)\right)dt, \tag{17}$$

$$\dot{\mathbf{x}}(t) = \mathbf{A}\mathbf{x}(t) + \mathbf{B}\mathbf{u}(t), \quad t\in\mathcal{T}, \ (\boldsymbol{\gamma}(t)), \tag{18}$$

$$\mathbf{C}^T\mathbf{x}(t) = D(t), \quad t\in\mathcal{T}, \ (\lambda(t)), \tag{19}$$

$$\underline{\mathbf{x}}(t) \le \mathbf{x}(t) \le \overline{\mathbf{x}}(t), \quad t\in\mathcal{T}, \ (\underline{\boldsymbol{\nu}}(t),\overline{\boldsymbol{\nu}}(t)), \tag{20}$$

$$\underline{\mathbf{u}}(t) \le \mathbf{u}(t) \le \overline{\mathbf{u}}(t), \quad t\in\mathcal{T}, \ (\underline{\boldsymbol{\mu}}(t),\overline{\boldsymbol{\mu}}(t)), \tag{21}$$

$$\mathbf{x}(0) = \mathbf{x}^0, \tag{22}$$

where J is the objective functional defined in (1), $F(\mathbf{x}(t))$ represents the total operation cost of the system, and $\mathbf{A}$ and $\mathbf{B}$ are respectively $(K+3R)\times(K+3R)$ and $(K+3R)\times(K+2R)$ matrices of parameters, defined as follows:

$$A = \begin{pmatrix} \mathbf{0} & \mathbf{0} & \mathbf{0} & \mathbf{0} \\ \mathbf{0} & \mathbf{0} & \mathbf{0} & \mathbf{0} \\ \mathbf{0} & \mathbf{0} & \mathbf{0} & \mathbf{0} \\ \mathbf{0} & -\boldsymbol{\eta}^{d^{-1}} & \boldsymbol{\eta}^c & \mathbf{0} \end{pmatrix}, B = \begin{pmatrix} \mathbf{I}_K & \mathbf{0} & \mathbf{0} \\ \mathbf{0} & \mathbf{I}_R & \mathbf{0} \\ \mathbf{0} & \mathbf{0} & \mathbf{I}_R \\ \mathbf{0} & \mathbf{0} & \mathbf{0} \end{pmatrix}, \tag{23}$$

where $\mathbf{I}_K$ and $\mathbf{I}_R$ are respectively identity matrices of orders K and R. The $(K+3R)$-dimensional vector $\mathbf{C}$ in (19) is defined as $\mathbf{C}=(\mathbf{1}_K;\mathbf{1}_R;-\mathbf{1}_R;\mathbf{0})$.

C. Derivation of Optimality Conditions

Here we intend to derive the necessary and sufficient optimality conditions for the continuous-time optimal control problem (17)-(22). Underlying assumptions for the derivations are: 1) the power trajectories $\mathbf{G}(t)$, $\mathbf{G}^s(t)$, $\mathbf{D}^s(t)$ are C^1 (continuously differentiable) functions of t; 2) the cost functions

are continuous and convex functions of their arguments; 3) the charging utility functions of ES devices are continuous and concave functions of their arguments; 4) the cost and utility functions are not explicit functions of t. Let us form the Hamiltonian and Lagrangian functions associated with problem (17)-(22) as:

$$\mathcal{H}\left(\mathbf{x}(t),\mathbf{u}(t),\boldsymbol{\gamma}(t)\right)=F(\mathbf{x}(t))+\boldsymbol{\gamma}^T(t)(\mathbf{A}\mathbf{x}(t)+\mathbf{B}\mathbf{u}(t))\,, \quad (24)$$

$$\begin{aligned}\mathcal{L}\big(\mathbf{x}(t),\mathbf{u}(t),\boldsymbol{\gamma}(t),\underline{\boldsymbol{\nu}}(t),\overline{\boldsymbol{\nu}}(t),\underline{\boldsymbol{\mu}}(t),\overline{\boldsymbol{\mu}}(t)\big)&=\mathcal{H}\left(\mathbf{x}(t),\mathbf{u}(t),\boldsymbol{\gamma}(t)\right)\\ &+\underline{\boldsymbol{\nu}}^T(t)(\underline{\mathbf{x}}(t)-\mathbf{x}(t))+\overline{\boldsymbol{\nu}}^T(t)(\mathbf{x}(t)-\overline{\mathbf{x}}(t))+\underline{\boldsymbol{\mu}}^T(t)(\underline{\mathbf{u}}(t)-\mathbf{u}(t))\\ &+\overline{\boldsymbol{\mu}}^T(t)(\mathbf{u}(t)-\overline{\mathbf{u}}(t))+\lambda(t)(D(t)-\mathbf{C}^T\mathbf{x}(t)). \quad (25)\end{aligned}$$

The Hamiltonian function in (24) is composed of two terms, where the first term is the instantaneous operation cost at time t, and the second term is the variations of the total operation cost over $\mathcal{T}$ with respect to the incremental changes in the state variables within an infinitesimal time interval starting from t. The optimality conditions are derived as follows [25]. For the sake of brevity, the arguments of Hamiltonian and Lagrangian functions are eliminated in the sequel.

1) Pontryagin Minimum Principle (PMP): The optimal control trajectories $\mathbf{u}^*(t)$ minimize the Hamiltonian:

$$\mathbf{u}^*(t)=\underset{\mathbf{u}(t)\in\psi(\mathbf{x}(t))}{\operatorname{argmin}}\left(\mathcal{H}\left(\mathbf{x}^*(t),\mathbf{u}(t),\boldsymbol{\gamma}^*(t)\right)\right), \quad (26)$$

where $\psi(\mathbf{x}(t))$ is the set of admissible controls that satisfy the constraints (18)-(22).

2) Adjoint Equations: For optimal pair $\mathbf{x}^*(t)$, $\mathbf{u}^*(t)$, the adjoint functions satisfy the following set of equations:

$$\begin{aligned}\dot{\boldsymbol{\gamma}}^*(t)=-\frac{\partial\mathcal{L}^*}{\partial\mathbf{x}(t)}&=-\frac{\partial F(\mathbf{x}^*(t))}{\partial\mathbf{x}(t)}-\mathbf{A}^T\boldsymbol{\gamma}^*(t)\\ &-\overline{\boldsymbol{\nu}}^*(t)+\underline{\boldsymbol{\nu}}^*(t)+\lambda^*(t)\mathbf{C}. \quad (27)\end{aligned}$$

3) First Order Conditions: For optimal pair $\mathbf{x}^*(t)$, $\mathbf{u}^*(t)$, the Lagrangian satisfies the following set of equations:

$$\frac{\partial\mathcal{L}^*}{\partial\mathbf{u}(t)}=\mathbf{B}^T\boldsymbol{\gamma}^*(t)+\overline{\boldsymbol{\mu}}^*(t)-\underline{\boldsymbol{\mu}}^*(t)=0. \quad (28)$$

4) Complimentarity Slackness: The complimentarity slackness conditions are as follows:

$$\underline{\nu}_i^*(t)(\underline{x}_i(t)-x_i^*(t))=0,\ \underline{\nu}_i^*(t)\geq 0,\ i=1,...,K+3R, \quad (29)$$
$$\overline{\nu}_i^*(t)(x_i^*(t)-\overline{x}_i(t))=0,\ \overline{\nu}_i^*(t)\geq 0,\ i=1,...,K+3R, \quad (30)$$
$$\underline{\mu}_i^*(t)(\underline{u}_i(t)-u_i^*(t))=0,\ \underline{\mu}_i^*(t)\geq 0,\ i=1,...,K+2R, \quad (31)$$
$$\overline{\mu}_i^*(t)(u_i^*(t)-\overline{u}_i(t))=0,\ \overline{\mu}_i^*(t)\geq 0,\ i=1,...,K+2R. \quad (32)$$

5) Jump Conditions: If a state trajectory $x_i(t)$ reaches its maximum or minimum limits at $t=\tau$, the associated adjoint function experiences discontinuities at this point, stated as:

$$\gamma_i^*(\tau^+)=\overline{\zeta}_i(\tau)-\underline{\zeta}_i(\tau)+\gamma_i^*(\tau^-),\qquad i=1,...,K+3R, \quad (33)$$
$$\overline{\zeta}_i(\tau)(x_i^*(\tau)-\overline{x}_i(\tau))=0,\ \overline{\zeta}_i(\tau)\geq 0,\ i=1,...,K+3R, \quad (34)$$
$$\underline{\zeta}_i(\tau)(\underline{x}_i(\tau)-x_i^*(\tau))=0,\ \underline{\zeta}_i(\tau)\geq 0,\ i=1,...,K+3R, \quad (35)$$

where $\overline{\zeta}_i(\tau)$ and $\underline{\zeta}_i(\tau)$ are the jump values, which are governed by (34) and (35). Note that the Hamiltonian (24) is continuous at the jump points.

6) Transversality Conditions: Optimal adjoint functions satisfy the following conditions at the end point of $\mathcal{T}$:

$$\gamma_i^*(T)=\overline{\alpha}_i-\underline{\alpha}_i,\qquad i=1,...,K+3R, \quad (36)$$
$$\overline{\alpha}_i(x_i^*(T)-\overline{x}_i(T))=0,\quad \overline{\alpha}_i\geq 0,\quad i=1,...,K+3R, \quad (37)$$
$$\underline{\alpha}_i(\underline{x}_i(T)-x_i^*(T))=0,\quad \underline{\alpha}_i\geq 0,\quad i=1,...,K+3R, \quad (38)$$

where $\overline{\alpha}_i$ and $\underline{\alpha}_i$ respectively equal to the values of Lagrange multiplier of the max and min limit constraints at $t=T$.

III. Continuous-time Marginal Price of Energy Generation and Storage

Marginal price is defined as the cost to serve the next increment of load in a system that is economically operated. In order to define the marginal price in our proposed continuous-time model, let the load trajectory $D(t)$ at time $t\in\mathcal{T}$ be incremented by an infinitesimally small localized C^1 trajectory, $\delta D(t)$, which is present in the incremental time interval from t to $t+\delta t$ and vanishes at the end points of the interval. This incremental variation is sufficiently small that an optimal solution still exists and involves the same binding inequality constraints. The incremental load variation $\delta D(t)$ results in incremental changes to the optimal state and control trajectories $\mathbf{x}^*(t)$ and $\mathbf{u}^*(t)$, as well as the total operation cost $F(\mathbf{x}^*(t))$. Let us define the *value function*, $V(\mathbf{x}^*(t))$, as the cost incurred when starting from state $\mathbf{x}^*(t)$ at time t and optimally control the system to the end of $\mathcal{T}$:

$$\begin{aligned}V(\mathbf{x}^*(t))&=\min_{\mathbf{u}(t')\in\psi(\mathbf{x}(t'))}\int_t^T F(\mathbf{x}(t'))dt'\\ &=\int_t^T\mathcal{L}^*dt',\quad\forall t\in\mathcal{T}, \quad (39)\end{aligned}$$

where $\mathcal{L}^*$ is the optimal value of the Lagrangian. The value function $V(\mathbf{x}^*(t))$ is a C^2 function of the state trajectories and a monotonically decreasing differentiable function of time. Thus, the rate of change in the optimal objective functional of (17)-(22) in infinitesimal time period δt is equal to the minus time derivative of the value function, i.e., $-\dot{V}(\mathbf{x}^*(t))=\mathcal{L}^*$. Hence, the rate at which the optimal objective functional changes due to an incremental change at load from time t to $t+\delta t$ would be the rate of change in the optimal Lagrangian (25) with respect to infinitesimal change in load at time t, i.e., $\frac{\partial\mathcal{L}^*}{\partial D(t)}$. In addition, let $\lambda^*(t)$ be the optimal Lagrange multiplier trajectory associated with the continuous-time power balance constraint (19). We characterize the continuous-time marginal price of energy generation and storage in the theorem below.

Theorem 1. *Consider the optimal control problem* (17)-(22). *For any optimal pair* $\mathbf{x}^*(t)$ *and* $\mathbf{u}^*(t)$, $\lambda^*(t)$ *given by:*

$$\lambda^*(t)=\frac{\partial\mathcal{L}^*}{\partial D(t)}\qquad\forall t\in\mathcal{T}, \quad (40)$$

is the continuous-time marginal price of energy generation and storage.

Proof. Let us calculate $\frac{\partial \mathcal{L}^*}{\partial D(t)}$ by taking partial derivative of the optimal Lagrangian (25) with respect to the load variation:

$$\begin{aligned}\frac{\partial \mathcal{L}^*}{\partial D(t)} &= \frac{\partial F(\mathbf{x}^*(t))}{\partial D(t)} + \frac{\partial \boldsymbol{\gamma}^{*T}(t)}{\partial D(t)}\left(\mathbf{A}\mathbf{x}^*(t) + \mathbf{B}\mathbf{u}^*(t)\right)\\ &+\boldsymbol{\gamma}^{*T}(t)\mathbf{A}\frac{\partial \mathbf{x}^*(t)}{\partial D(t)}+\boldsymbol{\gamma}^{*T}(t)\mathbf{B}\frac{\partial \mathbf{u}^*(t)}{\partial D(t)}+(\overline{\boldsymbol{\nu}}^*(t)-\underline{\boldsymbol{\nu}}^*(t))^T\frac{\partial \mathbf{x}^*(t)}{\partial D(t)}\\ &+\frac{\partial \overline{\boldsymbol{\nu}}^{*T}(t)}{\partial D(t)}(\mathbf{x}^*(t)-\overline{\mathbf{x}}(t))+\frac{\partial \underline{\boldsymbol{\nu}}^{*T}(t)}{\partial D(t)}(\underline{\mathbf{x}}(t)-\mathbf{x}^*(t))\\ &+\frac{\partial \overline{\boldsymbol{\mu}}^{*T}(t)}{\partial D(t)}(\mathbf{u}^*(t)-\overline{\mathbf{u}}(t))+\frac{\partial \underline{\boldsymbol{\mu}}^{*T}(t)}{\partial D(t)}(\underline{\mathbf{u}}(t)-\mathbf{u}^*(t))\\ &+\left(\overline{\boldsymbol{\mu}}^{*T}(t)-\underline{\boldsymbol{\mu}}^{*T}(t)\right)\frac{\partial \mathbf{u}^*(t)}{\partial D(t)}+\lambda^*(t)-\lambda^*(t)\mathbf{C}^T\frac{\partial \mathbf{x}^*(t)}{\partial D(t)}. \quad (41)\end{aligned}$$

Let us eliminate the zero terms in (41) applying the complimentarity slackness conditions, and rearrange the terms as:

$$\begin{aligned}\frac{\partial \mathcal{L}^*}{\partial D(t)} &= \lambda^*(t) + \frac{\partial \boldsymbol{\gamma}^{*T}(t)}{\partial D(t)}(\mathbf{A}\mathbf{x}^*(t) + \mathbf{B}\mathbf{u}^*(t))\\ &+\left(\mathbf{B}^T\boldsymbol{\gamma}^*(t)+\overline{\boldsymbol{\mu}}^*(t)-\underline{\boldsymbol{\mu}}^*(t)\right)^T\frac{\partial \mathbf{u}^*}{\partial D(t)}+\Big(\frac{\partial F(\mathbf{x}^*(t))}{\partial \mathbf{x}(t)}\\ &+\mathbf{A}^T\boldsymbol{\gamma}^*(t)+\overline{\boldsymbol{\nu}}^*(t)-\underline{\boldsymbol{\nu}}^*(t)-\lambda^*(t)\mathbf{C}\Big)^T\frac{\partial \mathbf{x}^*(t)}{\partial D(t)}. \quad (42)\end{aligned}$$

Making the following substitutions in (42), we derive (43): from (18), the state equation in the second term is replaced by $\dot{\mathbf{x}}^*(t)$; from (28), the third term equals to zero; finally from (27), the last term equals to $-\dot{\boldsymbol{\gamma}}^{*T}(t)\frac{\partial \mathbf{x}^*(t)}{\partial D(t)}$.

$$\begin{aligned}\frac{\partial \mathcal{L}^*}{\partial D(t)} &=\lambda^*(t)+\frac{\partial \boldsymbol{\gamma}^{*T}(t)}{\partial D(t)}\dot{\mathbf{x}}^*(t)-\dot{\boldsymbol{\gamma}}^{*T}(t)\frac{\partial \mathbf{x}^*(t)}{\partial D(t)}\\ &=\lambda^*(t)+\big(\frac{\partial \boldsymbol{\gamma}^*(t)}{\partial \mathbf{x}^*(t)}\frac{\partial \mathbf{x}^*(t)}{\partial D(t)}\big)^T\dot{\mathbf{x}}^*(t)-\dot{\boldsymbol{\gamma}}^{*T}(t)\frac{\partial \mathbf{x}^*(t)}{\partial D(t)}\\ &=\lambda^*(t)+\big(\frac{\partial \mathbf{x}^*(t)}{\partial D(t)}\big)^T\frac{\partial \boldsymbol{\gamma}^*(t)}{\partial \mathbf{x}^*(t)}\dot{\mathbf{x}}^*(t)-\dot{\boldsymbol{\gamma}}^{*T}(t)\frac{\partial \mathbf{x}^*(t)}{\partial D(t)}\\ &=\lambda^*(t)+\left(\dot{\boldsymbol{\gamma}}^{*T}(t)-\dot{\boldsymbol{\gamma}}^{*T}(t)\right)\frac{\partial \mathbf{x}^*(t)}{\partial D(t)}\\ &=\lambda^*(t). \quad (43)\end{aligned}$$

The term $\frac{\partial \boldsymbol{\gamma}^*(t)}{\partial \mathbf{x}^*(t)}$ in (43) is the symmetric Hessian matrix of the value function, so it is equal to its transpose in the third line. This concludes the proof. □

IV. Calculation of the Continuous-time Price

Here we aim to derive closed-form formulas for the continuous-time marginal price in Theorem 1. We start from (41) where the vectors $\frac{\partial \mathbf{x}(t)}{\partial D(t)}$ and $\frac{\partial \mathbf{u}(t)}{\partial D(t)}$ are the generation and ramping variations of generating units and ES devices contributing towards balancing the load variation $\delta D(t)$. In $\frac{\partial \mathbf{x}(t)}{\partial D(t)}$, the elements associated with capacity-constrained units and ES devices are zero, while in $\frac{\partial \mathbf{u}(t)}{\partial D(t)}$ both capacity- and ramp-constrained units/devices take zero values. Accordingly, by applying the complimentarity slackness conditions (29)-(32), and for $\mathbf{C}^T\frac{\partial \mathbf{x}(t)}{\partial D(t)}$ equals 1, we recast (41) as [1]:

$$\lambda(t) = \frac{\partial \mathcal{L}}{\partial D(t)} = \frac{\partial F(\mathbf{x}(t))}{\partial D(t)} + \frac{\partial(\boldsymbol{\gamma}^T(t)\dot{\mathbf{x}}(t))}{\partial D(t)}. \quad (44)$$

[1]For notational simplicity we drop asterisks from optimal trajectories

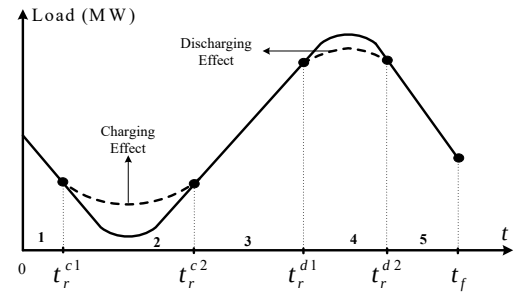

Fig. 1. Hypothetical ES charge-discharge cycle

Three cases of marginal prices are calculated in subsections below for three combinations of marginal generating units and ES devices over $\mathcal{T}$, as shown in Fig. 1 for an ES charge-discharge cycle on a hypothetical load profile.

A. Case 1: Generating Units Set the Marginal Price

Consider a set of time intervals denoted by $\mathcal{T}_1^s$ when no ES device is either charging or discharging, and one or more generating units set the marginal price (e.g., intervals 1, 3, 5 in Fig. 1). In this case, the vectors of state and control variables only include elements associated with generating units, i.e., $\mathbf{x}(t) = (\mathbf{G}(t); \mathbf{0}; \mathbf{0}; \mathbf{0})$ and $\mathbf{u}(t) = (\dot{\mathbf{G}}(t); \mathbf{0}; \mathbf{0})$. Substituting the value of $\frac{\partial(\boldsymbol{\gamma}^T(t)\dot{\mathbf{x}}(t))}{\partial D(t)}$ from Appendix A in (44) and expanding $\frac{\partial F(\mathbf{x}(t))}{\partial D(t)}$, we calculate $\lambda(t)$ in Case 1 as:

$$\begin{aligned}\lambda(t) = &\sum_{k\in(K_t^u\cup K_t^r)} IC_k^G(t)\frac{\partial G_k(t)}{\partial D(t)}\\ &+\sum_{k\in K_t^r}\left(\underline{\dot{\mu}}_k^G(t)-\overline{\dot{\mu}}_k^G(t)\right)\frac{\partial G_k(t)}{\partial D(t)}, \quad t\in\mathcal{T}_1^s, \quad (45)\end{aligned}$$

where K_t^u and K_t^r are sets of unconstrained and ramp-constrained units at time t, and $IC_k^G(t) \triangleq \frac{\partial C^G(G_k(t))}{\partial G_k(t)}$ is the incremental cost rate of unit k. In the special case with a single unconstrained marginal unit, the price in (45) would be equal to the incremental cost rate of the unit, which is consistent with the traditional pricing models [26].

B. Case 2: Generating Units and ES Devices in Charging State Set the Marginal Price

Consider a set of time intervals denoted by $\mathcal{T}_2^s$ when in addition to generating units, one or more ES devices contribute to supplying the load variation by changing their *charging* power and ramping (e.g., interval 2 in Fig. 1). In this case: $\mathbf{x}(t) = (\mathbf{G}(t); \mathbf{0}; \mathbf{D}^s(t); \mathbf{E}^s(t))$ and $\mathbf{u}(t) = (\dot{\mathbf{G}}(t); \mathbf{0}; \dot{\mathbf{D}}^s(t))$. Substituting $\frac{\partial(\boldsymbol{\gamma}^T(t)\dot{\mathbf{x}}(t))}{\partial D(t)}$ from Appendix A in (44) and expanding $\frac{\partial F(\mathbf{x}(t))}{\partial D(t)}$, we calculate $\lambda(t)$ in Case 2 as follows:

$$\begin{aligned}\lambda(t) = &\sum_{k\in(K_t^u\cup K_t^r)} IC_k^G(t)\frac{\partial G_k(t)}{\partial D(t)}\\ &+\sum_{k\in K_t^r}\left(\underline{\dot{\mu}}_k^G(t)-\overline{\dot{\mu}}_k^G(t)\right)\frac{\partial G_k(t)}{\partial D(t)}\\ &-\sum_{r\in(R_t^u\cup R_t^r)} IU_r^S(t)\frac{\partial D_r^s(t)}{\partial D(t)}\\ &+\sum_{r\in R_t^r}\left(\underline{\dot{\mu}}_r^{s,D}(t)-\overline{\dot{\mu}}_r^{s,D}(t)\right)\frac{\partial D_r^s(t)}{\partial D(t)}, t\in\mathcal{T}_2^s, \quad (46)\end{aligned}$$

where R_t^u and R_t^r are sets of unconstrained and ramp-constrained ES devices at time t, and $IU_r^S(t)$ is the *incremental charging cost rate of ES device* r defined as:

$$IU_r^S(t) \triangleq \frac{\partial U^S\left(D_r^s(t)\right)}{\partial D_r^s(t)} - \eta_r^c \gamma_r^{s,E}(t_r^{c1}), \quad t \in \mathcal{T}_2^s, \tag{47}$$

where $\gamma_r^{s,E}(t_r^{c1})$ is the value of adjoint function associated with the ES state equation (5) at the start of charging interval, which is derived in (88) in Appendix A.

C. Case 3: Generating Units and ES Devices in Discharging State Set the Marginal Price

Consider a set of time intervals denoted by $\mathcal{T}_3^s$ when in addition to generating units, one or more ES devices contribute to supplying the load variation by changing their *discharging* power and ramping (e.g., interval 4 in Fig. 1). In this case: $\mathbf{x}(t) = (\mathbf{G}(t); \mathbf{G}^s(t); \mathbf{0}; \mathbf{E}^s(t))$ and $\mathbf{u}(t) = (\dot{\mathbf{G}}(t); \dot{\mathbf{G}}^s(t); \mathbf{0})$. Substituting the value of $\frac{\partial(\boldsymbol{\gamma}^T(t)\dot{\mathbf{x}}(t))}{\partial D(t)}$ from Appendix A in (44) and expanding $\frac{\partial F(\mathbf{x}(t))}{\partial D(t)}$, we calculate $\lambda(t)$ in Case 3 as follows:

$$\begin{aligned}\lambda(t) = &\sum_{k \in (K_t^u \cup K_t^r)} IC_k^G(t) \frac{\partial G_k(t)}{\partial D(t)} \\ &+ \sum_{k \in K_t^r} \left(\underline{\dot{\mu}}_k^G(t) - \overline{\dot{\mu}}_k^G(t)\right) \frac{\partial G_k(t)}{\partial D(t)} \\ &+ \sum_{r \in (R_t^u \cup R_t^r)} IC_r^S(t) \frac{\partial G_r^s(t)}{\partial D(t)} \\ &+ \sum_{r \in R_t^r} \left(\underline{\dot{\mu}}_r^{s,G}(t) - \overline{\dot{\mu}}_r^{s,G}(t)\right) \frac{\partial G_r^s(t)}{\partial D(t)}, \quad t \in \mathcal{T}_3^s,\end{aligned} \tag{48}$$

where $IC_r^S(t)$ is the *incremental discharging cost rate of ES device* r defined as:

$$IC_r^S(t) = \frac{\partial C^S(G_r^s(t))}{\partial G_r^s(t)} - \frac{1}{\eta_r^d} \gamma_r^{s,E}(t_r^{d1}), \tag{49}$$

where $\gamma_r^{s,E}(t_r^{d1})$ is derived in (92) in Appendix A.

Definition 1 (Net Incremental Surplus of Stored Energy)**.** *The adjoint function $\gamma_r^{s,E}(t)$ associated with the ES state equation* (5) *represents the net surplus of incremental change in the energy stored at ES device r at time t, and is defined as the net incremental surplus of stored energy (NISSE).*

The *NISSE* calculated in (88) at the start of ES charging is equal to the utility of charging one MW of power from the grid per unit of time (defined through charging utility function) minus the marginal price at that time, divided by the charging efficiency of the ES device. For instance, for an ES device with the charging utility function variation of $\$20/MW$ per unit of time and charging efficiency of 0.9, the *NISSE* at a marginal price of $\$15/MW$ per unit of time would equal to 5.55, meaning that the ES device would gain $\$5.55$ for each MW of power stored per unit of time. It is shown in Appendix A that the value of *NISSE* is set at the start of charging and discharging intervals and stay constant during both intervals. As in (50), the constant value of *NISSE* during charging and discharging intervals would be the same if the ES device does not reach its energy capacity limit at the end of the charging interval. However, when an ES device is fully charged, *NISSE* experiences a constant jump at the start of discharging interval that equals to integral of the Lagrange multiplier $\overline{\nu}_r^{s,E}(t)$ from the end of charging interval to the start of discharging interval (see (50)). This is consistent with the jump condition (33).

At the end of discharging interval, the energy stored in ES device may reach its minimum limit. The value of *NISSE* after that is calculated below by taking the integral of the adjoint equation associated with the energy trajectory in (27):

$$\gamma_r^{s,E}(t) = \gamma_r^{s,E}(t_r^{d2}) + \int_{t_r^{d2}}^{t} \underline{\nu}_r^{s,E}(t')dt', \quad \forall t > t_r^{d2}. \tag{50}$$

D. Observations

The closed-form marginal price formulas in (45), (46) and (48) lead us to extract the following important results and observations on ES scheduling and pricing in power systems.

Observation 1. *Impact of Ramping on Marginal Price*: The continuous-time marginal price, derived in closed-form in (45), (46), and (48), explicitly show that when a generating unit or ES device reaches its ramping limit, time derivative of Lagrange multiplier associated with the binding ramping constraint appears in the price formula, causing a price increase that reflects the shortage of ramping in the system.

Observation 2. *Start of Charging Condition for ES Devices*: The incremental charging utility rate in (47) at the start of charging equals to the marginal price at that time, meaning that an ES device starts charging when the incremental charging utility rate intersects with the marginal price trajectory.

Observation 3. *Start of Discharging Condition for ES Devices*: an ES device starts discharging when its incremental discharging cost rate intersects with the marginal price trajectory. In order to show this, let us expand the adjoint equation of discharging power trajectory of ES device r at the start of discharging t_r^{d1}, by substituting $\dot{\gamma}_r^{s,G}(t)$ from (28) in (27):

$$\begin{aligned}\overline{\dot{\mu}}_r^{s,G}(t_r^{d1}) - \underline{\dot{\mu}}_r^{s,G}(t_r^{d1}) = &\frac{\partial C^S(G_r^s(t))}{\partial G_r^s(t)}\Big|_{t=t_r^{d1}} \\ &- \frac{\gamma_r^{s,E}(t_r^{d1})}{\eta_r^d} - \lambda(t_r^{d1}),\end{aligned} \tag{51}$$

where $\overline{\dot{\mu}}_r^{s,G}(t_r^{d1})$ and $\underline{\dot{\mu}}_r^{s,G}(t_r^{d1})$ are zero, as the C^1 continuity of discharging power trajectory requires the ES devices to start discharging with zero ramp, and the first two terms in the right-hand-side of (51) are equal to the incremental discharging cost rate (49) at the start of discharging interval.

Observation 4. *Composition of Incremental Charging/ Discharging Utility/Cost Rates*: The incremental charging utility rate of ES device r defined in (47), indicates the utility of charging one MW of power per unit of time into ES device r. The incremental charging utility rate depends on the charging utility function variation, minus the *NISSE* of ES device r during charging times the charging efficiency of the ES device.

The incremental discharging cost rate of ES device r defined in (49), indicates the cost of discharging one MW of power per unit of time from ES device r. The incremental discharging

cost rate depends on the discharging cost function variation, minus the *NISSE* of ES device r during discharging divided by the discharging efficiency of the ES device. Note that the incremental discharging cost rate would also experience a jump when the ES device reaches its maximum capacity at the end of charging interval. This means that the energy stored in the constrained ES device is valued more in the system by having greater incremental discharging cost rate. In turn, the increased incremental discharging cost rate of energy-constrained ES device impacts the marginal price trajectory during the discharging interval through (48).

Observation 5. *ES with Zero Charging/Discharging Utility/Cost Functions*: In case the ES charging utility function is zero, the incremental charging utility rate in (47) would be a constant value equaling to the marginal electricity price at time t_r^{c1}. In case both ES charging utility and discharging cost functions are zero, the incremental discharging cost rate would be a constant value equal to:

$$IC_r^S(t)=\frac{\lambda(t_r^{c2})}{\eta_r^d\eta_r^c}+\frac{1}{\eta_r^d}\int_{t_r^{c2}}^{t_r^{d1}}\bar{\nu}_r^{s,E}(t)dt,\quad t\in\mathcal{T}_3^s. \tag{52}$$

V. Computational Solution of Continuous-time Scheduling and Pricing Problems

The proposed model for continuous-time scheduling of energy generation and storage in (17)-(22) is a continuous-time optimal control problem with infinite dimensional decision space that is computationally intractable. Here we intend to leverage our previous works in [22], [27], and develop a function space-based solution method for the proposed problem. The proposed solution method is based on reducing the dimensionality of the continuous-time decision and parameter trajectories by modeling them in a finite-order function space spanned by Bernstein polynomials. The Bernstein polynomials of degree Q include $Q+1$ polynomials defined as [28], [29]:

$$b_{q,Q}(t)=\binom{Q}{q}t^q(1-t)^{Q-q},\quad t\in[0,1). \tag{53}$$

Let us first subdivide the scheduling horizon $\mathcal{T}$ into M intervals $\mathcal{T}_m=[t_m,t_{m+1}),\rightarrow\ \mathcal{T}=\cup_{m=0}^{M-1}\mathcal{T}_m$, with lengths $T_m=t_{m+1}-t_m$, and then construct a subset of basis functions formed by the Bernstein polynomials of degree Q in each interval $\mathcal{T}_m$, forming a spline function space to represent the whole scheduling horizon $\mathcal{T}$. Thus, the vector of basis functions $\mathbf{e}^{(Q)}(t)=(e_1^{(Q)}(t),\ldots,e_P^{(Q)}(t))^T$ spanning the whole $\mathcal{T}$ contains $P=(Q+1)M$ functions with components defined as:

$$e_{m(Q+1)+q}^{(Q)}(t)=b_{q,Q}\left(\frac{t-t_m}{T_m}\right),t\in[t_m,t_{m+1}), \tag{54}$$

for $m=0,\ldots,M-1;q=0,\ldots,Q$. To reduce the notation, we define $p\equiv m(Q+1)+q$, where p goes from 0 to $(Q+1)M-1$. In the following, we present different components of the proposed solution method.

A. Modeling the Operational Constraints of Generating Units

Let us project the generation trajectories of generating units, $\mathbf{G}(t)$, in the Bernstein function space $\mathbf{e}^{(Q)}(t)$ defined in (54):

$$\mathbf{G}(t)=\mathbf{G}\mathbf{e}^{(Q)}(t), \tag{55}$$

where $\mathbf{G}$ is a $K\times P$ matrix of Bernstein coefficients associated with the generation trajectories of generating units. Modeling generation ramping trajectory, as well as capacity and ramping constraints, continuity constraints, and generation cost function in the Bernstein function space are presented in [22], [27]. In this paper, we focus below on modeling ES operation constraints in the function space and refer the readers to [22], [27] for details on modeling generating units.

B. Modeling the Operational Constraints of Energy Storage

Let us project the charging and discharging power trajectories of ES devices in the space spanned by $\mathbf{e}^{(Q)}(t)$:

$$\mathbf{D}^s(t)=\mathbf{D}^s\mathbf{e}^{(Q)}(t),\qquad \mathbf{G}^s(t)=\mathbf{G}^s\mathbf{e}^{(Q)}(t), \tag{56}$$

where $\mathbf{D}^s=(\mathbf{D}_1^s;\cdots;\mathbf{D}_R^s)$ and $\mathbf{G}^s=(\mathbf{G}_1^s;\cdots;\mathbf{G}_R^s)$ are $R\times P$ matrices of Bernstein coefficients of charging and discharging power trajectories, with the row vectors $\mathbf{D}_r^s$ and $\mathbf{G}_r^s$ indicating the Bernstein coefficients of ES device r. In the following, multiple properties of Bernstein polynomials are leveraged to model ES ramping and energy trajectory, as well as the operational constraints and cost functions, while ensuring continuity of trajectories.

1) Modeling ES Ramping Trajectory: The time derivatives of Bernstein polynomials of degree Q can be expressed as a linear combination of two Bernstein polynomials of degree $Q-1$ [28]. This property enables defining the continuous-time ramping trajectories of ES devices in the space spanned by the Bernstein polynomials of degree $Q-1$ as:

$$\dot{\mathbf{D}}^s(t)=\mathbf{D}^s\dot{\mathbf{e}}^{(Q)}(t)=\mathbf{D}^s\boldsymbol{\mathcal{M}}\mathbf{e}^{(Q-1)}(t)=\dot{\mathbf{D}}^s\mathbf{e}^{(Q-1)}(t), \tag{57}$$

$$\dot{\mathbf{G}}^s(t)=\mathbf{G}^s\dot{\mathbf{e}}^{(Q)}(t)=\mathbf{G}^s\boldsymbol{\mathcal{M}}\mathbf{e}^{(Q-1)}(t)=\dot{\mathbf{G}}^s\mathbf{e}^{(Q-1)}(t), \tag{58}$$

where $\mathcal{M}$ is the $P\times(P-M)$ matrix relating $\dot{\mathbf{e}}^{(Q)}(t)$ and $\mathbf{e}^{(Q-1)}(t)$, and $\dot{\mathbf{D}}^s$ and $\dot{\mathbf{G}}^s$ are $R\times(P-M)$ matrices of Bernstein coefficients associated with ES charge and discharge ramping trajectories, linearly related with the Bernstein coefficients of the corresponding ES power trajectories as:

$$\dot{\mathbf{D}}^s=\mathbf{D}^s\boldsymbol{\mathcal{M}},\qquad \dot{\mathbf{G}}^s=\mathbf{G}^s\boldsymbol{\mathcal{M}}. \tag{59}$$

2) Modeling ES Energy Trajectory: The integral of Bernstein polynomials of degree Q are linearly related to Bernstein polynomials of degree $Q+1$, suggesting that there is a $P\times(P+M)$ linear mapping, $\boldsymbol{\mathcal{N}}$, relating the integral of $\mathbf{e}^{(Q)}(t)$ with $\mathbf{e}^{(Q+1)}(t)$. Using this property and integrating the state equation (5) over t, we derive the projection of ES energy trajectories in Bernstein function space:

$$\begin{aligned}\mathbf{E}^s(t)&=\mathbf{E}^{s,0}+(\boldsymbol{\eta}^c\mathbf{D}^s-\boldsymbol{\eta}^{d^{-1}}\mathbf{G}^s)\int_0^t\mathbf{e}^{(Q)}(t')dt'\\&=\mathbf{E}^{s,0}+(\boldsymbol{\eta}^c\mathbf{D}^s-\boldsymbol{\eta}^{d^{-1}}\mathbf{G}^s)\boldsymbol{\mathcal{N}}\mathbf{e}^{(Q+1)}(t)\\&=\left(\mathbf{E}^{s,0}\mathbf{1}_{P+M}+\left(\boldsymbol{\eta}^c\mathbf{D}^s-\boldsymbol{\eta}^{d^{-1}}\mathbf{G}^s\right)\boldsymbol{\mathcal{N}}\right)\mathbf{e}^{(Q+1)}(t)\\&=\mathbf{E}^s\mathbf{e}^{(Q+1)}(t),\end{aligned} \tag{60}$$

where $\mathbf{E}^{s,0}\mathbf{1}_{P+M}^T$ in the third line is the projection of constant initial energy values vector $\mathbf{E}^{s,0}$ to the space spanned by $\mathbf{e}^{(Q+1)}(t)$, and $\mathbf{E}^s$ is a $R\times(P+M)$ matrix of Bernstein coefficients of ES energy trajectories, which is equal to:

$$\mathbf{E}^s=\mathbf{E}^{s,0}\mathbf{1}_{P+M}+\left(\boldsymbol{\eta}^c\mathbf{D}^s-\boldsymbol{\eta}^{d^{-1}}\mathbf{G}^s\right)\boldsymbol{\mathcal{N}}. \tag{61}$$

3) Continuity of Energy, Power and Ramping Trajectories: The optimality conditions of the optimal control problem (17)-(22) requires C^1 continuity of the charging and discharging power trajectories of ES devices. In order to ensure the C^1 continuity requirement at the interval connection points, we impose continuity constraints on the Bernstein coefficients of adjacent intervals as follows:

$$G^s_{r,m(Q+1)+Q} = G^s_{r,(m+1)(Q+1)},\ m = 0, \dots M-1, \tag{62}$$

$$D^s_{r,m(Q+1)+Q} = D^s_{r,(m+1)(Q+1)},\ m = 0, \dots M-1, \tag{63}$$

$$\frac{1}{T_m}\big(G^s_{r,m(Q+1)+Q} - G^s_{r,m(Q+1)+Q-1}\big) = \frac{1}{T_{m+1}}\big(G^s_{r,(m+1)(Q+1)+1} - G^s_{r,(m+1)(Q+1)}\big),\quad m = 0, \dots M-1, \tag{64}$$

$$\frac{1}{T_m}\big(D^s_{r,m(Q+1)+Q} - D^s_{r,m(Q+1)+Q-1}\big) = \frac{1}{T_{m+1}}\big(D^s_{r,(m+1)(Q+1)+1} - D^s_{r,(m+1)(Q+1)}\big),\quad m = 0, \dots M-1. \tag{65}$$

4) Inequality Constraints on Energy, Power and Ramping Trajectories: The convex hull property of the Bernstein polynomials allows us to efficiently impose inequality constraints on the energy, power and ramping trajectories of ES devices. More specifically, let $\mathcal{R}$ be the control polygon formed by the Bernstein coefficients $\mathbf{E}^s_r$ of the continuous-time energy trajectory of ES device r in the space spanned by $\mathbf{e}^{(Q+1)}(t)$. The convex hull property states that the energy trajectory $E^s_r(t)$ will never be outside of the convex hull of the control polygon $\mathcal{R}$. This means that the minimum and maximum of the Bernstein coefficients in interval m represent the lower and upper bound for the continuous-time energy trajectories within that interval. Therefore, the continuous-time inequality constraints on the energy trajectories can be imposed by limiting the Bernstein coefficients at each interval:

$$\underline{E}^s_r \le E^s_{r,m(Q+2)+q} \le \overline{E}^s_r, \qquad \forall q, \forall m, \forall r. \tag{66}$$

where $\underline{E}^s_r$ and $\overline{E}^s_r$ are respectively the minimum and maximum energy capacity of ES device r. Similar constraints apply for charging and discharging power trajectories, as well as ramping trajectories for imposing the associated continuous-time power and ramping constraints.

5) Modeling ES Utility/Cost Functions: Assume that the charging utility and discharging cost functions of the ES devices are respectively concave and convex nonlinear functions of the charging and discharging power trajectories. Here we propose a model to linearize the nonlinear utility and cost functions. The linear utility and cost functions may be also utilized for market participation of ES devices where the ES devices submit multiple price-quantity pairs for charging and discharging. As shown in Fig. 2, let us divide the charging power capacity of ES device r to N^D_r segments using the intermediate points $d^s_{r,0} = 0, d^s_{r,1}, \dots, d^s_{r,N^D_r} = \overline{D}^s_r$, and the discharging power capacity to N^G_r segments using the intermediate points $g^s_{r,0} = 0, g^s_{r,1}, \dots, g^s_{r,N^G_r} = \overline{G}^s_r$. We define positive continuous-time auxiliary variables $v_{r,h}(t)$ and $w_{r,j}(t)$ to respectively model charging and discharging power

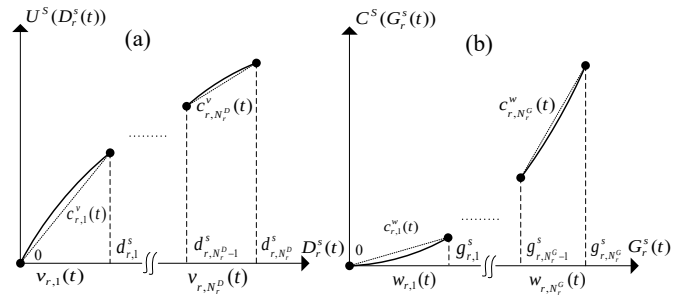

Fig. 2. Linearization of (a) charging utility function, (b) discharging cost function

trajectories of ES device r as follows:

$$D^s_r(t) = \sum_{h=1}^{N^D_r} v_{r,h}(t) = \mathbf{1}^T_{N^D_r}\mathbf{V}_r(t), \tag{67}$$

$$G^s_r(t) = \sum_{j=1}^{N^G_r} w_{r,j}(t) = \mathbf{1}^T_{N^G_r}\mathbf{W}_r(t), \tag{68}$$

where $\mathbf{V}_r(t)$ and $\mathbf{W}_r(t)$ are respectively N^D_r- and N^G_r-dimensional vectors of auxiliary variables associated with charging and discharging power trajectories and $\mathbf{1}_{N^D_r}$ and $\mathbf{1}_{N^G_r}$ are respectively N^D_r- and N^G_r-dimensional vectors of ones. We approximate the nonlinear charging utility and discharging cost functions $U^S\big(D^s_r(t)\big)$ and $C^S\big(G^s_r(t)\big)$ with the linearized cost functions $\hat{U}^S\big(\mathbf{V}_r(t)\big)$ and $\hat{C}^S\big(\mathbf{W}_r(t)\big)$ written in terms of the auxiliary variables as follows:

$$U^S\big(D^s_r(t)\big) \approx \hat{U}^S\big(\mathbf{V}_r(t)\big) = \sum_{h=1}^{N^D_r} c^v_{r,h}(t) v_{r,h}(t), \tag{69}$$

$$C^S\big(G^s_r(t)\big) \approx \hat{C}^S\big(\mathbf{W}_r(t)\big) = \sum_{j=1}^{N^G_r} c^w_{r,j}(t) w_{r,j}(t), \tag{70}$$

where $c^v_{r,h}(t)$ and $c^w_{r,j}(t)$ are respectively charging and discharging cost coefficients. In order to model the linear functions $\hat{U}^S\big(\mathbf{V}_r(t)\big)$ and $\hat{C}^S\big(\mathbf{W}_r(t)\big)$ in the Bernstein function space, we expand the auxiliary variables in the space spanned by the Bernstein basis function of degree Q as follows:

$$v_{r,h}(t) = \mathbf{v}_{r,h}\mathbf{e}^{(Q)}(t), \qquad w_{r,j}(t) = \mathbf{w}_{r,j}\mathbf{e}^{(Q)}(t), \tag{71}$$

where $\mathbf{v}_{r,h}$ and $\mathbf{w}_{r,j}$ are the vectors of Bernstein coefficients. Using (67) and (68), the Bernstein coefficients of charging and discharging power trajectories relate to the Bernstein coefficients of the corresponding auxiliary variables by:

$$\mathbf{D}^s_r = \sum_{h=1}^{N^D_r} \mathbf{v}_{r,h}, \qquad \mathbf{G}^s_r = \sum_{j=1}^{N^G_r} \mathbf{w}_{r,j}, \tag{72}$$

where $\mathbf{G}^s_r$ and $\mathbf{D}^s_r$ are respectively the rth rows of the matrices $\mathbf{G}^s$ and $\mathbf{D}^s$ defined in (56). The Bernstein coefficients of auxiliary variables are constrained to their limits as:

$$0 \le \mathbf{v}_{r,h} \ \le \big(d^s_{r,h} - d^s_{r,h-1}\big)\,\mathbf{1}_P,\ \forall r,\ \forall h, \tag{73}$$

$$0 \le \mathbf{w}_{r,j} \le \big(g^s_{r,j} - g^s_{r,j-1}\big)\,\mathbf{1}_P,\quad \forall r,\ \forall j. \tag{74}$$

where $\mathbf{1}_P$ is a P-dimensional vector of ones. Substituting the Bernstein representations of auxiliary variables from (71) in (69) and (70), and integrating the right-hand-sides over $\mathcal{T}$, we calculate the linear charging utility and discharging cost functions of ES device r over $\mathcal{T}$ in terms of the Bernstein representation of auxiliary variables as:

$$\int_{\mathcal{T}} \hat{U}^S\big(\mathbf{V}_r(t)\big)dt = \sum_{m=0}^{M-1} \frac{T_m}{Q+1} \sum_{h=1}^{N_r^D} c_{r,h,m}^v \sum_{q=0}^{Q} v_{r,h,m(Q+1)+q}, \tag{75}$$

$$\int_{\mathcal{T}} \hat{C}^S\big(\mathbf{W}_r(t)\big)dt = \sum_{m=0}^{M-1} \frac{T_m}{Q+1} \sum_{j=1}^{N_r^G} c_{r,j,m}^w \sum_{q=0}^{Q} w_{r,j,m(Q+1)+q}, \tag{76}$$

where the cost coefficients $c_{r,h,m}^v \equiv c_{r,h}^v(t_m)$ and $c_{r,j,m}^w \equiv c_{r,j}^w(t_m)$ are constant within each interval m.

C. Modeling Power Balance Constraint

Let the load trajectory be spanned over the Bernstein function space of degree Q as:

$$D(t) = \mathbf{D}\mathbf{e}^{(Q)}(t), \tag{77}$$

where $\mathbf{D}$ is a P-dimensional row vector of Bernstein coefficients. Substituting the Bernstein models of generation, charging and discharging power trajectories from (55)-(56) and load trajectory from (77) in the continuous-time power balance constraint (6), we derive:

$$\left(\mathbf{1}_K^T\mathbf{G} + \mathbf{1}_R^T\mathbf{G}^s - \mathbf{1}_R^T\mathbf{D}^s\right)\mathbf{e}^{(Q)}(t) = \mathbf{D}\mathbf{e}^{(Q)}(t). \tag{78}$$

Eliminating $\mathbf{e}^{(Q)}(t)$ from both sides, we have:

$$\mathbf{1}_K^T\mathbf{G} + \mathbf{1}_R^T\mathbf{G}^s - \mathbf{1}_R^T\mathbf{D}^s = \mathbf{D}, \tag{79}$$

that converts the continuous-time power balance constraint (6) to algebraic equations on the Bernstein coefficients.

In summary, the proposed model for ES devices in this section, plus the power balance equation (79), along with the model for generating units presented in Section V of [22] present the proposed function space-based solution method that converts the continuous-time problem (1)-(14) into a MILP problem with the Bernstein coordinates of decision trajectories as variables.

Note that the function space in (54) includes $\mathbf{e}^{(0)}(t)$ that is formed by the Bernstein polynomials of degree 0 and models the piecewise constant trajectories associated with the traditional discrete-time scheduling models. Accordingly, the proposed function space-based method includes, as a special case, the discrete-time hourly model by choosing the Bernstein polynomials of degree 0 as the function space.

VI. Numerical Results

This section presents the numerical results of implementing the proposed continuous-time scheduling and pricing models on the IEEE RTS [30] with 32 generating units. The Bernstein polynomials of degree 3 are used to simulate the continuous-time model. The five-minute real-time load forecast data of CAISO for Feb. 4, 2016 are scaled down to the IEEE-RTS peak load of 2850MW, and used to calculate the coefficients of Bernstein polynomials of degree 3 associated with the continuous-time load trajectory using the three-point finite difference method in [29]. The load data of the hourly model is also calculated as the mid-points of the hourly intervals of the calculated continuous-time load. The resulting continuous-time and hourly load profiles are shown in Fig. 3 and utilized in the simulations. Three cases are studied:

- Study 1: System operation without ES;
- Study 2: System operation with operator-owned ES;
- Study 3: Market-based system operation with ES.

For each study, we simulate and compare the day-ahead operation of IEEE-RTS using the continuous-time model and the traditional hourly model. The study cases were solved using CPLEX 12.6.2 on a desktop computer with a 4.0GHz i7 processor and 32GB of RAM. The computation times are respectively 0.549, 0.447, and 0.485 seconds for studies 1-3 using the hourly model, and 1.536, 0.947, and 1.209 seconds using the continuous-time model.

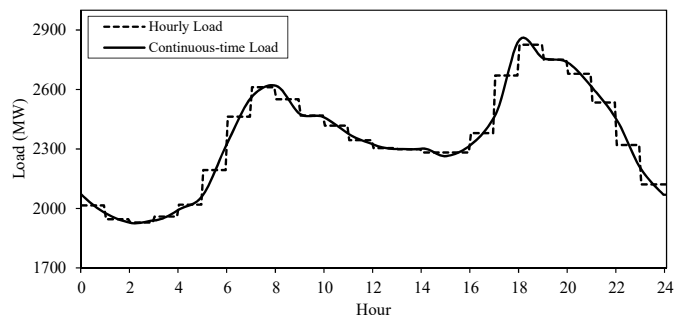

Fig. 3. Continuous-time and hourly net-load profile

A. Study 1: System Operation without Energy Storage

The day-ahead operation of IEEE-RTS without any ES device is studied here. The day-ahead operation costs of the system using the proposed continuous-time method and the hourly model equal to $\$461,006.4$ and $\$459,746.2$, respectively. The operation cost of the continuous-time model is higher than that of the hourly model, as the proposed model dispatches more energy to supply the continuous-time variations of load in day-ahead operation. In addition, the continuous-time model commits an additional 20MW unit at the peak load of hour 18 to supply the additional ramping requirement captured by the continuous-time load model. This is neglected by the hourly model, where the 20MW unit is not committed.

B. Study 2: System operation with Operator-owned ES

The day-ahead operation of IEEE-RTS with the addition of an ES device is studied here. The energy capacity, power rating, and ramping rate of the ES device are respectively 1200MWh, 250MW, and 25MW/min, and the charge and discharge efficiency of the ES device are both 90%. This ES could be a large ES device (e.g., pumped hydro storage), or represent an aggregation of multiple utility-scale battery energy storage. In this study, we consider a non-market power system operation environment, where the operator owns and

operates the ES device, and the charging utility and discharging cost functions are assumed to be zero. The day-ahead operation costs associated with the continuous-time and hourly models, as well as the associated cost savings as compared to study 1, are provided in Table I. In Table I, the operation of ES device reduces the operation cost using both models, but the continuous-time model yields greater cost saving for the IEEE-RTS than the hourly model.

TABLE I
DAY-AHEAD IEEE-RTS OPERATION COSTS – STUDY 2

	Hourly Model		Continuous-time Model	
	Operation Cost ($)	Cost Saving Compared to Case 1 ($)	Operation Cost ($)	Cost Saving Compared to Case 1 ($)
Study 2	449,246.7	10,499.5	450,041.3	10,965.1

Generation Schedule: The schedule of generating units in the proposed continuous-time model in studies 1 and 2 are compared in Fig. 4. In Fig. 4.(b), ES utilization in study 2 modifies the schedule of generating units compared to study 1, as the proposed model co-optimizes the day-ahead operation of ES devices and generating units. Further, ES utilization reduces cycling of the generating units in off-peak hours 1-6, and eliminates the need for committing expensive 197MW and 20MW units respectively during the peak hours 8 and 18.

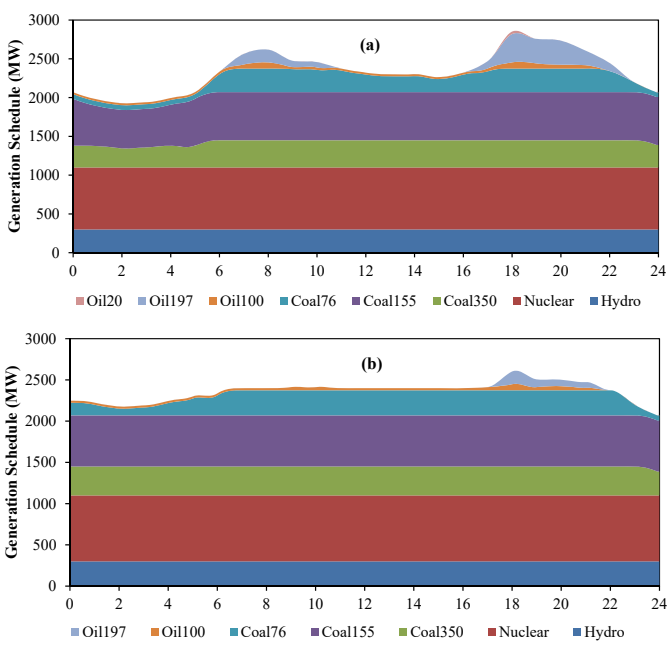

Fig. 4. Continuous-time schedule of generating units: (a) study 1,(b) study 2

ES schedule and incremental rates: The optimal energy, power and ramping trajectories of the ES device in study 2 using both the hourly and continuous-time models are shown in Figs. 5. In addition, Fig. 6 shows the associated ES incremental charging utility rate, incremental discharging cost rate, as well as the *NISSE* in the proposed continuous-time model. In Fig. (5).(b), the negative and positive powers are respectively associated with the ES charging and discharging states, where both the hourly and continuous-time models schedule two charge-discharge cycles for the ES device. The charging and discharging cycles are respectively shown in light and dark shades in Fig. 6. Note that in Fig. 5.(c) the hourly model does not generate ramping trajectory, while the proposed continuous-time model explicitly schedules for continuous-time ramping trajectory of the ES devices.

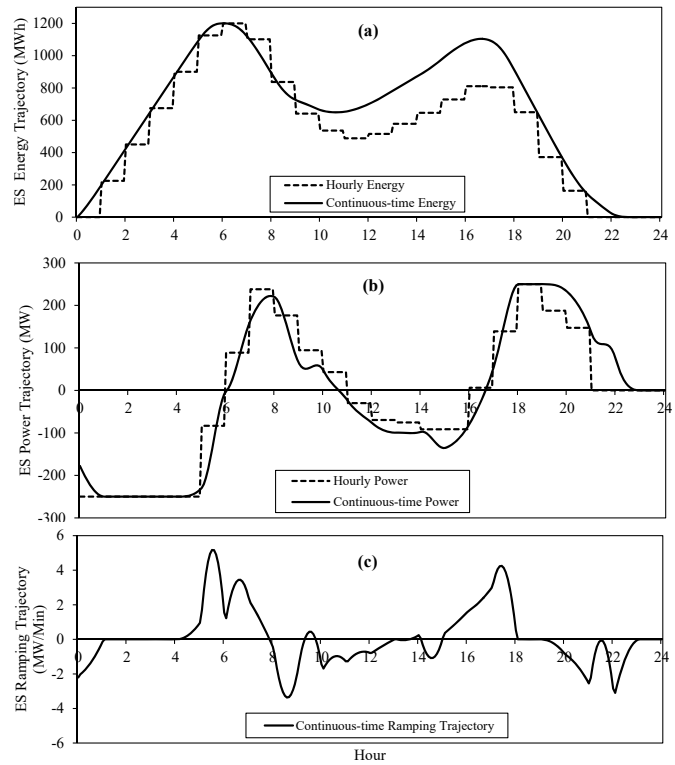

Fig. 5. Continuous-time and hourly ES energy, power and ramping trajectories in study 2: (a) Energy trajectory, (b) Power trajectory, (c) Ramping trajectory.

The first charging cycle starts at hour 0, and the ES device is fully charged by the end of hour 6. As described in Observation 2, the incremental charging utility rate of ES device in Fig. 6 equals to the system marginal price at the start of charging, i.e., $\$13.9/MW$ per unit of time. The *NISSE* of ES device at $t = 0$ is calculated using (88) as $\gamma^{s,E}(0) = -\frac{13.9}{0.9} = -15.4$. As discussed in Section IV, the incremental charging utility rate and *NISSE* remain constant during the entire charging interval. As ES devices reaches its maximum energy capacity at the end of hour 6, the *NISSE* experiences a jump of 2.6 that equals to the Lagrange multiplier of the maximum energy capacity constraint (see (92)). Thus, *NISSE* reaches to -18.0 $(= -15.4 - 2.6)$ at hour 7 when the ES device starts discharging energy back to the grid until hour 11. During discharging interval of hours 7-11, the incremental discharging cost rate is calculated from (49) as $-\frac{-18.0}{0.9} = \$20.0/MW$ per unit of time, and remains constant during the interval.

The second charge-discharge cycle starts at hour 12 by charging the ES device until hour 17, but the ES device does not get fully charged in this cycle. The ES starts discharging immediately to supply the second load peak at hour 18, and fully discharges by hour 23. Using the same formulas as described for the first cycle, the incremental charging utility and incremental discharging cost rates are respectively calculated as $\$16.2/MW$ and $\$20.0/MW$ per unit of time. The *NISSE* remains constant during the second charge-discharge cycle as the ES device does not reach its energy capacity.

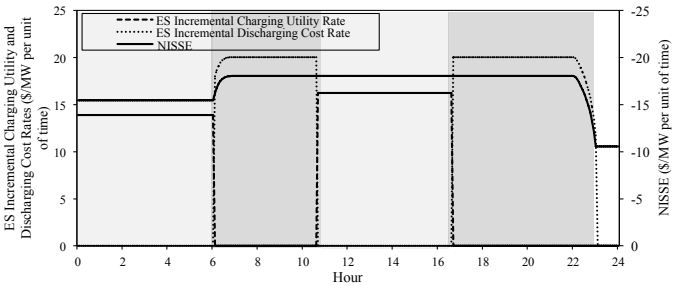

Fig. 6. ES Incremental charging utility and discharging cost rates and the *NISSE* in Study 2. The light and dark shades respectively show the ES charging and discharging cycles.

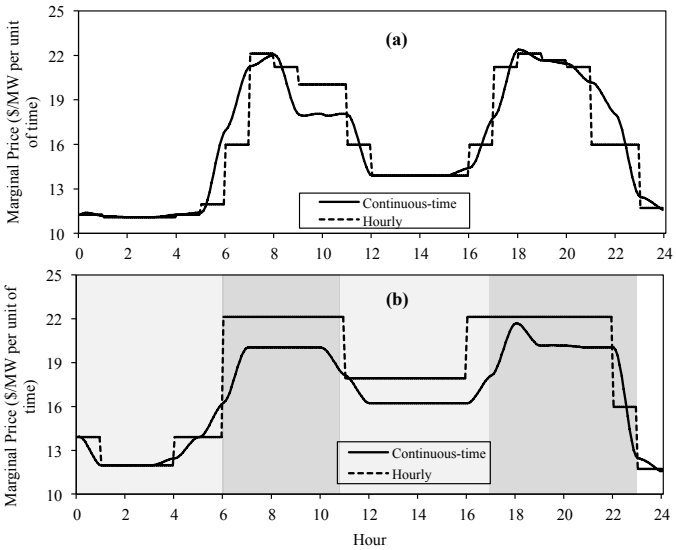

Fig. 7. Marginal prices in (a) Study 1, (b) Study 2. The light and dark shades respectively show the ES charging and discharging cycles.

Marginal Price: The continuous-time and hourly marginal prices for studies 1 and 2 are shown in Figs. 7. In Figs. 7, the continuous-time marginal price reflects the continuous-time variation of load and generation schedules, while the hourly model provide a constant price for each hour that is not sensitive to the sub-hourly load variations. As shown in Fig. 7.(b), ES utilization in study 2 modifies the marginal prices in both continuous-time and hourly models, as compared to the prices for study 1 shown in Fig. 7.(a), where the prices solely depend on the marginal prices of generating units.

As discussed in detail in Section IV, three different combination of generating units and ES devices contribute in the calculation of marginal prices in Fig. 7.(b): *1) Generating units set the price*: during hours 2-5 and 18-20, the ES device respectively charges and discharges at its maximum power rating and generating units set the marginal price. *2) ES device set the price while charging*: during hours 7-10 and 21, all generating units are capacity-constrained and the ES device sets the marginal price in charging state. As derived in (46), the price at these hours equals to the incremental charging utility rate of the ES device that is equal to $\$20.0/MW$ per unit of time. *3) ES device set the price while discharging*: during hours 12-16, generating units are capacity-constrained and the ES device sets the marginal price in discharging state. As derived in (48), the price at these hours equals to the incremental discharging cost rate of the ES device that is equal to $\$16.2/MW$ per unit of time. *4) A combination of generating units and ES device set the price*: during other hours of the scheduling horizon, a combination of ES device and various generating units provide the incremental load and set the marginal price calculated using (46) and (48).

C. Study 3: Market-based System Operation with ES

In this study, we consider the market-based operation of the IEEE-RTS where ES devices are allowed to submit bids to charge and discharge in the market. The same ES device in Study 2 submits two charging offers and two discharging bids with the data provided in Table II. The generation bids of generating units are the same as their incremental cost rates in [30]. The day-ahead operation costs for the continuous-time and hourly models, as well as the associated cost savings compared to study 1 are provided in Table III. The cost savings in study 3 are lower than those in study 2, yet, the continuous-time model bears more cost saving than the hourly model.

TABLE II
ES CHARGING UTILITY AND DISCHARGING COST FUNCTION

Charging Power Segments (MW)	$0 \le D^s(t) \le 125$	$125 < D^s(t) \le 250$
Charging Offers ($/MW per unit of time)	10.5	10
Discharging Power Segments (MW)	$0 \le G^s(t) \le 125$	$125 < G^s(t) \le 250$
Discharging Bids ($/MW per unit of time)	18.5	19

TABLE III
DAY-AHEAD IEEE-RTS OPERATION COSTS – STUDY 3

	Hourly Model		**Continuous-time Model**	
	Operation Cost ($)	**Cost Saving Compared to Case 1 ($)**	**Operation Cost ($)**	**Cost Saving Compared to Case 1 ($)**
Study 3	456,430.5	3,315.7	457,129.4	3,876.9

ES schedule and incremental rates: The optimal energy, power, and ramping trajectories of the ES device in study 3 are shown in Fig. 8. In addition, Fig. 9 shows the ES incremental charging utility rate, incremental discharging cost rate, as well as the *NISSE* in the proposed continuous-time model. In Figs. 8, ES utilization is reduced in the market-based environment, when the charging offers and discharging bids of the ES device may not always be competitive in the market. The ES device gets charged only once during hours 0-6 and discharged during two intervals of hours 7-11 and 17-23 in order to supply the two peak loads. The ES stays idle during hours 12-16.

In study 3, the incremental charging utility and discharging cost rates in Fig. 9 are not constant during the intervals, as the charging utility and discharging cost functions are varying in two segments as in Table II. At $t=0$, where the ES is charging at segment 2, the incremental charging utility rate in Fig. 9 equals to the marginal price of $\$12.2/MW$ per unit of time. Using (88), *NISSE* is calculated as $\gamma^{s,E}(0)=\frac{-1}{0.9}(12.2-10)=-2.4$, and remains constant during the entire charging interval. At hour 5, the ES charging power falls below 125MW and the charging offer increases to $\$10.5/MW$ per unit of time. Thus, the value of incremental charging utility rate in Fig. 9 increases to $\$12.7/MW$ per unit of time. ES device finishes charging at hour 6 without reaching its maximum energy so *NISSE* stays constant during discharging. During discharging interval of hours 7-11 and 17-23 in Fig. 9, the incremental

discharging cost rate is calculated from (49), which equals to either $\$21.2/MW$ or $\$21.7/MW$ per unit of time, depending on discharging power and the associated bid.

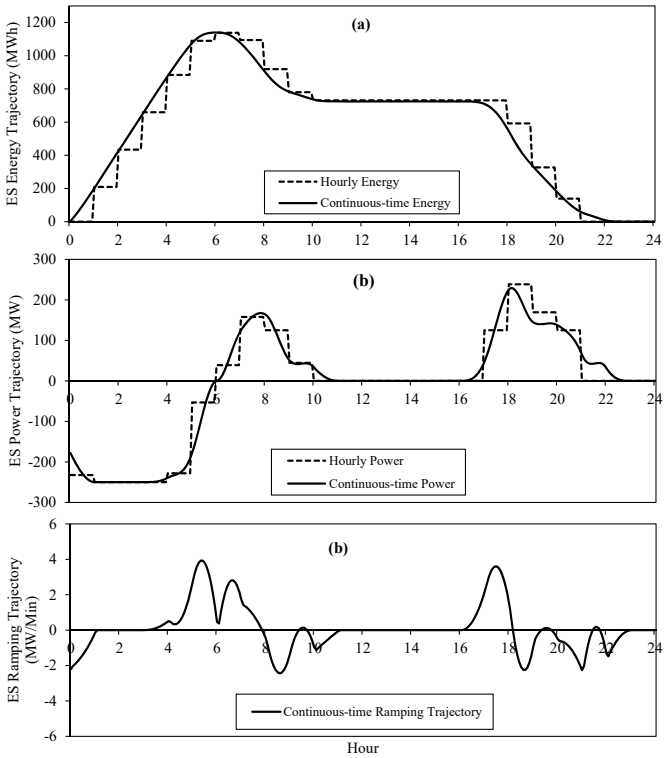

Fig. 8. Continuous-time and hourly ES energy, power and ramping trajectories in study 3: (a) Energy trajectory, (b) Power trajectory, (c) Ramping trajectory.

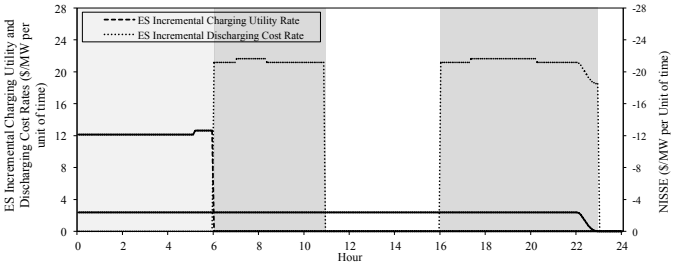

Fig. 9. ES Incremental charging utility and discharging cost rates and the *NISSE* in Study 3.

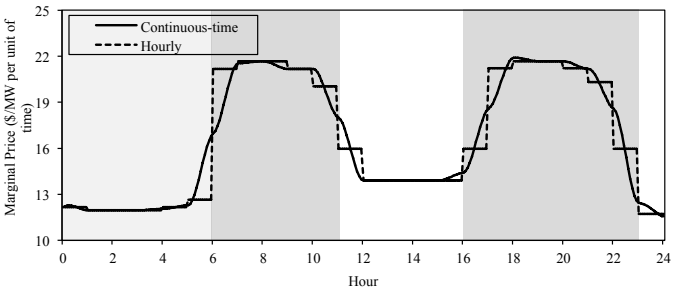

Fig. 10. Marginal prices in Study 3.

Marginal Price: The continuous-time and hourly marginal prices in study 3 are shown in Fig. 10. In this study, the marginal prices in Fig. 10 belong to the following two cases: *1) Generating units set the price*: during hours 2-4 when the ES device charges at its maximum power rating, and during hours 12-16 and 24 when the ES device is idle, generating units set the marginal price. *2) A combination of generating unit(s) and ES device are marginal*: during other hours of the scheduling horizon, a combination of ES device at charging or discharging states and various generating units set the marginal price using the price formulas (46) and (48).

Impact of ES charging offers and discharging bids: The simulations are repeated for different values of changes in the charging offers and discharging bids as compared to the values given in Table II, and the system operation cost savings are compared in Fig. 11, where the zero changes corresponds to the results in Study 3. In Fig. 11, the cost savings of ES utilization increases when we increase the charging offers and decrease the discharging bids. More cost savings are achieved in Fig. 11.(b) using the continuous-time model.

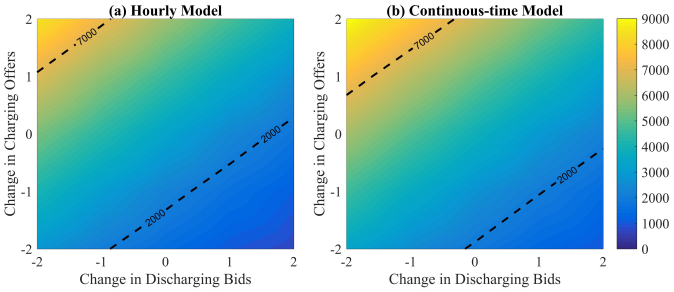

Fig. 11. System operation cost savings of ES utilization for different cost and utility functions using (a) hourly model, (b) continuous-time model.

VII. Conclusions

This paper presented a fundamental model for continuous-time scheduling and pricing of generating units and ES devices in power systems operation. We first presented the proposed scheduling and pricing problems and the associated optimality conditions, and derived the closed-form formulas for calculating continuous-time marginal price of energy generation and storage, which lead us to extract important observations on ES scheduling and pricing in power systems. We also proposed a novel method for solving the proposed continuous-time problem. The proposed solution method ensures the optimality of the solutions by maintaining the continuity of the decision trajectories, and uniquely schedules for continuous-time energy, power and ramping trajectories of the ES devices and captures their ultimate flexibility to supply the continuous-time net-load variations.

Using the simulations conducted on the IEEE-RTS, it was observed that the ES operation in both market-based and traditional system operation would reduce the operation costs as well as ramping and cycling of the generating units, and would eliminate the need for committing expensive peaking units in the system. The benefits are more prominent in traditional operation where the operator schedules the ES device for the benefit of whole system. The ES operation may bring lower benefits to the system in market-based setting where the ES bids may not be competitive as compared to the generating units. The results confirm the derived closed-from price formulas and demonstrate in detail that the operation of

ES devices creates an intertemporal dependence in marginal prices, where the marginal price during ES discharging has a direct relationship with the marginal price of the times when the ES is charged. It is also demonstrated that the ES device may become marginal during charging or discharging and set the marginal prices that are calculated using the incremental charging utility and discharging cost rates of the ES device.

Future works include expanding the proposed model and include different ancillary services that may be provided by ES devices in electricity market operation. Further, model extensions include the consideration of transmission network equations and constraints and development of price formulas for locational marginal price in the presence of ES devices. Developing the stochastic model that accounts for the net-load uncertainty in the proposed problem is also in order.

Appendix A

The goal here is to calculate the value of term $\frac{\partial(\boldsymbol{\gamma}^T(t)\dot{\mathbf{x}}(t))}{\partial D(t)}$ in (44) for the three cases of price derivation in Section IV:

1) Case 1: In Case 1, $\mathbf{x}(t) = (\mathbf{G}(t); \mathbf{0}; \mathbf{0}; \mathbf{0})$, $\mathbf{u}(t) = (\dot{\mathbf{G}}(t); \mathbf{0}; \mathbf{0})$, so the term $\frac{\partial(\boldsymbol{\gamma}^T(t)\dot{\mathbf{x}}(t))}{\partial D(t)}$ is written as:

$$\frac{\partial(\boldsymbol{\gamma}^T(t)\dot{\mathbf{x}}(t))}{\partial D(t)} = \frac{\partial(\boldsymbol{\gamma}^{G^T}(t)\dot{\mathbf{G}}(t))}{\partial D(t)}. \tag{80}$$

In order to calculate $\frac{\partial(\boldsymbol{\gamma}^{G^T}(t)\dot{\mathbf{G}}(t))}{\partial D(t)}$, we multiply the first order condition associated with the generation trajectories in (28) with $\dot{\mathbf{G}}(t)$ and take derivative with respect to $D(t)$ as below:

$$\frac{\partial(\boldsymbol{\gamma}^{G^T}(t)\dot{\mathbf{G}}(t))}{\partial D(t)} = \left(\underline{\dot{\boldsymbol{\mu}}}^G(t) - \overline{\ddot{\boldsymbol{\mu}}}^G(t)\right)^T \frac{\partial \mathbf{G}(t)}{\partial D(t)}. \tag{81}$$

2) Case 2: In Case 2, $\mathbf{x}(t) = (\mathbf{G}(t); \mathbf{0}; \mathbf{D}^s(t); \mathbf{E}^s(t))$, $\mathbf{u}(t) = (\dot{\mathbf{G}}(t); \mathbf{0}; \dot{\mathbf{D}}^s(t))$, so the term $\frac{\partial(\boldsymbol{\gamma}^T(t)\dot{\mathbf{x}}(t))}{\partial D(t)}$ becomes:

$$\frac{\partial(\boldsymbol{\gamma}^T(t)\dot{\mathbf{x}}(t))}{\partial D(t)} = \frac{\partial(\boldsymbol{\gamma}^{G^T}(t)\dot{\mathbf{G}}(t))}{\partial D(t)} + \frac{\partial(\boldsymbol{\gamma}^{s,D^T}(t)\dot{\mathbf{D}}^s(t))}{\partial D(t)} + \frac{\partial(\boldsymbol{\gamma}^{s,E^T}(t)\dot{\mathbf{E}}^s(t))}{\partial D(t)}, \tag{82}$$

where the first term is the same as (81), and with similar approach in deriving (81), the second term is calculated as:

$$\frac{\partial(\boldsymbol{\gamma}^{s,D^T}(t)\dot{\mathbf{D}}^s(t))}{\partial D(t)} = \left(\underline{\dot{\boldsymbol{\mu}}}^{s,D}(t) - \overline{\ddot{\boldsymbol{\mu}}}^{s,D}(t)\right)^T \frac{\partial \mathbf{D}^s(t)}{\partial D(t)}. \tag{83}$$

In order to calculate the third term in (82), we substitute $\dot{\mathbf{E}}^s(t)$ from the state equation (5):

$$\frac{\partial(\boldsymbol{\gamma}^{s,E^T}(t)\dot{\mathbf{E}}^s(t))}{\partial D(t)} = \frac{\partial\left(\boldsymbol{\gamma}^{s,E^T}(t)\boldsymbol{\eta}^c\mathbf{D}^s(t)\right)}{\partial D(t)}, \tag{84}$$

where we argue that $\boldsymbol{\gamma}^{s,E}(t)$ is constant during the charging state according to the adjoint equation of the energy trajectories in (27) and that the Lagrange multipliers $\underline{\boldsymbol{\nu}}^{s,E}(t)$ and $\overline{\boldsymbol{\nu}}^{s,E}(t)$ are zeros:

$$\dot{\boldsymbol{\gamma}}^{s,E}(t) = \underline{\boldsymbol{\nu}}^{s,E}(t) - \overline{\boldsymbol{\nu}}^{s,E}(t) = \mathbf{0} \rightarrow \boldsymbol{\gamma}^{s,E}(t) \equiv \text{Constant}. \tag{85}$$

Thus, (84) can be written as:

$$\frac{\partial(\boldsymbol{\gamma}^{s,E^T}(t)\dot{\mathbf{E}}^s(t))}{\partial D(t)} = \boldsymbol{\gamma}^{s,E^T}(t)\boldsymbol{\eta}^c\frac{\partial \mathbf{D}^s(t)}{\partial D(t)}. \tag{86}$$

The constant value of $\gamma_r^{s,E}(t)$ is calculated below at the start of charging interval (t_r^{c1} in Fig. 1) by using the adjoint equation of the charging power trajectory in (27) and substituting the value of $\dot{\gamma}_r^{s,D}(t)$ from (28):

$$\gamma_r^{s,E}(t_r^{c1}) = \frac{1}{\eta_r^c}\left(\frac{\partial U^S\left(D_r^s(t)\right)}{\partial D_r^s(t)}\Big|_{t=t_r^{c1}} - \lambda(t_r^{c1}) + \overline{\ddot{\mu}}_r^{s,D}(t_r^{c1}) - \underline{\dot{\mu}}_r^{s,D}(t_r^{c1})\right), \tag{87}$$

where $\underline{\dot{\mu}}_r^{s,D}(t_r^{c1})$ and $\overline{\ddot{\mu}}_r^{s,D}(t_r^{c1})$ are zero, as the C^1 continuity of charging power trajectories requires the ES devices to start and finish charging with zero ramp. Thus, $\gamma_r^{s,E}(t_r^{c1})$ is calculated as follows:

$$\gamma_r^{s,E}(t_r^{c1}) = \frac{1}{\eta_r^c}\left(\frac{\partial U^S(D_r^s(t))}{\partial D_r^s(t)}\Big|_{t=t_r^{c1}} - \lambda(t_r^{c1})\right). \tag{88}$$

3) Case 3: In Case 3, $\mathbf{x}(t) = (\mathbf{G}(t); \mathbf{G}^s(t); \mathbf{0}; \mathbf{E}^s(t))$, $\mathbf{u}(t) = (\dot{\mathbf{G}}(t); \dot{\mathbf{G}}^s(t); \mathbf{0})$, and the term $\frac{\partial(\boldsymbol{\gamma}^T(t)\dot{\mathbf{x}}(t))}{\partial D(t)}$ becomes:

$$\frac{\partial(\boldsymbol{\gamma}^T(t)\dot{\mathbf{x}}(t))}{\partial D(t)} = \frac{\partial(\boldsymbol{\gamma}^{G^T}(t)\dot{\mathbf{G}}(t))}{\partial D(t)} + \frac{\partial(\boldsymbol{\gamma}^{s,D^T}(t)\dot{\mathbf{G}}^s(t))}{\partial D(t)} + \frac{\partial(\boldsymbol{\gamma}^{s,E^T}(t)\dot{\mathbf{E}}^s(t))}{\partial D(t)}, \tag{89}$$

where the first term is the same as (81), and with similar approach in deriving (81), the second term is calculated as:

$$\frac{\partial(\boldsymbol{\gamma}^{s,D^T}(t)\dot{\mathbf{G}}^s(t))}{\partial D(t)} = \left(\underline{\dot{\boldsymbol{\mu}}}^{s,G}(t) - \overline{\ddot{\boldsymbol{\mu}}}^{s,G}(t)\right)^T \frac{\partial \mathbf{G}^s(t)}{\partial D(t)}. \tag{90}$$

In order to calculate the third term in (89), we substitute $\dot{\mathbf{E}}^s(t)$ from the state equation (5), assuming $\boldsymbol{\gamma}^{s,E}(t)$ is constant with the same reasoning as in Case 2:

$$\frac{\partial(\boldsymbol{\gamma}^{s,E^T}(t)\dot{\mathbf{E}}^s(t))}{\partial D(t)} = -\boldsymbol{\gamma}^{s,E^T}(t)\boldsymbol{\eta}^{d-1}\frac{\partial \mathbf{G}^s(t)}{\partial D(t)}, \tag{91}$$

In order to calculate the constant value of $\gamma_r^{s,E}(t)$ for ES device r during the discharging period, we calculate the change in the value of $\gamma_r^{s,E}(t)$ during the transition from the end of charging period t_r^{c2} to the start of discharging period t_r^{d1}, by taking the integral of the adjoint equation associated with the energy trajectory of ES device r in (27) during the transition:

$$\gamma_r^{s,E}(t_r^{d1}) = \gamma_r^{s,E}(t_r^{c2}) - \int_{t_r^{c2}}^{t_r^{d1}} \left(\overline{\nu}_r^{s,E}(t)\right) dt, \tag{92}$$

where the Lagrange multiplier associated with the minimum energy limit is eliminated (since ES devices cannot be discharged at their minimum energy limit).

REFERENCES

[1] "Grid energy storage," U.S. Department of Energy, December 2013.
[2] "Energy storage requirements for achieving 50% solar photovoltaic energy penetration in california," National Renewable Energy Laboratory, August 2016.
[3] "Quadrennial energy review second installment: Transforming the nation's electricity system," U.S. Department of Energy, January 2017.
[4] "Frequency regulation compensation in the organized wholesale power markets (order no. 755)," Federal Energy Regulatory Commission, 2011.
[5] "Electric storage participation in markets operated by regional transmission organizations and independent system operators; (notice of proposed rulemaking)," Federal Energy Regulatory Commission, 2016.
[6] "Advancing and maximizing the value of energy storage technology: A california roadmap," California ISO, 2014.
[7] "Energy storage and distributed energy resources stakeholder initiative: Revised draft final proposal," California ISO, 2016.
[8] "Energy storage: Market integration and optimization," New York ISO, 2016.
[9] "Business practices manual: Energy and operating reserve markets," Midcontinent ISO, 2016.
[10] "Energy storage study miso, policy studies," Midcontinent ISO, 2014.
[11] Y. Chen, M. Keyser, M. H. Tackett, and X. Ma, "Incorporating short-term stored energy resource into midwest iso energy and ancillary service market," *IEEE Trans. Power Systems*, vol. 26, no. 2, pp. 829–838, 2011.
[12] "How energy storage can participate in new england's wholesale electricity markets," New England Independent System Operator, 2016.
[13] H. Oh, "Optimal planning to include storage devices in power systems," *IEEE Trans. Power Systems*, vol. 26, no. 3, pp. 1118–1128, 2011.
[14] M. Parvania, M. Fotuhi-Firuzabad, and M. Shahidehpour, "Comparative hourly scheduling of centralized and distributed storage in day-ahead markets," *IEEE Trans. Sustainable Energy*, vol. 5, no. 3, pp. 729–737, 2014.
[15] Y. Ye, D. Papadaskalopoulos, and G. Strbac, "An mpec approach for analysing the impact of energy storage in imperfect electricity markets," in *13th International Conference on European Energy Market*, 2016.
[16] K. Bruninx, Y. Dvorkin, E. Delarue, H. Pandžić, W. D'haeseleer, and D. S. Kirschen, "Coupling pumped hydro energy storage with unit commitment," *IEEE Trans. Sustainable Energy*, vol. 7, no. 2, pp. 786–796, 2016.
[17] Y. Wen, C. Guo, H. Pandzic, and D. S. Kirschen, "Enhanced security-constrained unit commitment with emerging utility-scale energy storage," *IEEE Trans. Power Systems*, vol. 31, no. 1, pp. 652–662, 2016.
[18] C. O'Dwyer, L. Ryan, and D. Flynn, "Efficient large-scale energy storage dispatch: Challenges in future high renewables systems," *IEEE Trans. Power Systems*, 2017.
[19] M. Abdurrahman, S. Baker, B. Keshavamurthy, and M. Jacobs, "Energy storage as a transmission asset," *PJM Interconnection and Xtreme Power, Tech. Rep*, 2012.
[20] J. Taylor, "Financial storage rights," *IEEE Trans. Power Systems*, vol. 30, no. 2, pp. 997–1005, 2015.
[21] M. Parvania, M. Fotuhi-Firuzabad, and M. Shahidehpour, "Demand response participation in wholesale energy markets," in *Proc. IEEE Power and Energy Society General Meeting*, 2012, pp. 1–4.
[22] M. Parvania and A. Scaglione, "Unit commitment with continuous-time generation and ramping trajectory models," *IEEE Transactions on Power Systems*, vol. 31, no. 4, pp. 3169–3178, 2016.
[23] R. P. O'Neill, P. M. Sotkiewicz, B. F. Hobbs, M. H. Rothkopf, and W. R. Stewart, "Efficient market-clearing prices in markets with non-convexities," *European journal of operational research*, vol. 164, no. 1, pp. 269–285, 2005.
[24] M. Parvania and R. Khatami, "Continuous-time marginal pricing of electricity," *IEEE Transactions on Power Systems*, vol. 32, no. 3, pp. 1960–1969, 2017.
[25] A. Seierstad and K. Sydsaeter, *Optimal control theory with economic applications*. Elsevier North-Holland, Inc., 1986.
[26] A. J. Wood and B. F. Wollenberg, *Power generation, operation, and control*. John Wiley & Sons, 2012.
[27] M. Parvania and A. Scaglione, "Generation ramping valuation in day-ahead electricity markets," in *49th Hawaii International Conference on System Sciences (HICSS)*, 2016, pp. 2335–2344.
[28] P. Dierckx, *Curve and surface fitting with splines*. Oxford University Press, Inc., 1993.
[29] P. M. Prenter *et al.*, *Splines and variational methods*. Courier Corporation, 2008.
[30] R. T. S. T. Force, "The ieee reliability test system-1996," *IEEE Trans. Power Systems*, vol. 14, no. 3, pp. 1010–1020, 1999.

Roohallah Khatami (S' 2015) received the B.S. degree from Iran University of Science and Technology, Tehran, Iran, in 2007, and the M.S. degree from Amirkabir University of Technology, Tehran, Iran, in 2013, both in electrical engineering. He is currently working towards Ph.D. degree at the University of Utah. His research interests include power systems operation and electricity markets.

Masood Parvania (M' 2014) is currently an Assistant Professor of Electrical and Computer Engineering at the University of Utah. Dr. Parvania serves as an Associate Editor of the IEEE Transactions on Smart Grid and the IEEE Power Engineering Letters, and is the Chair of IEEE Power and Energy Society (PES) Utah Chapter, Chair of the IEEE PES Task Force on Reliability Impacts of Demand Response Integration, and the Vice-Chair of the IEEE PES Bulk Power Systems Operation Subcommittee. His research interests include the operation and planning of power and energy systems, and modeling and integration of distributed energy resources.

Pramod P. Khargonekar received BTech degree in Electrical Engineering from the Indian Institute of Technology, Bombay, India and M.S. degree in mathematics and Ph.D. degree in Electrical Engineering from the University of Florida. He has served in faculty positions at the University of Minnesota and The University of Michigan. He was Chairman of the Department of Electrical Engineering and Computer Science at Michigan from 1997 to 2001, and also held the title Claude E. Shannon Professor of Engineering Science there. From 2001 to 2009, he was Dean of the College of Engineering and the Eckis Professor Electrical and Computer Engineering at the University of Florida. He served as Deputy Director for Technology at the U.S. Department of Energy?s Advanced Research Projects Agency - Energy (ARPA-E). From March 2103 till June 2016, he served at the U.S. National Science Foundation as Assistant Director for Engineering. He is currently Vice Chancellor for Research and Distinguished Professor of Electrical Engineering and Computer Science at the University of California, Irvine. His current research interests are focused on renewable energy and electric grid, neural engineering, and systems and control theory. He is a recipient of the NSF Presidential Young Investigator Award, the American Automatic Control Council?s Donald Eckman Award, the Japan Society for Promotion of Science Fellowships, and a Distinguished Alumnus Award and Distinguished Service Award from the Indian Institute of Technology, Bombay. He is a co-recipient of the IEEE W.R.G. Baker Prize Award, the IEEE CSS George S. Axelby Best Paper Award, and the AACC Hugo Schuck Best Paper Award. He was a Springer Professor at the University of California, Berkeley in 2010. He is a Fellow of IEEE and IFAC. He has been on the list of Web of Science Highly Cited Researchers (2001).